Supplemental Material can be found at:
http://www.jbc.org/content/suppl/2008/12/23/M806928200.DC1.html
http://www.jbc.org/content/suppl/2009/02/19/284.9.5592.DC1.html

MEF2 pathway is used for insulin-like growth factor-induced myogenin expression (54). Huddleson *et al.* (42) have also shown that induction of KLF2 by shear stress requires a PI3K/chromatin-remodeling pathway. In contrast to our result, they claimed that AKT is not involved in this pathway, although it is activated by shear stress. We propose the involvement of AKT in Angl-mediated KLF2 induction because 1) AKT inhibitor and knockdown of AKT both inhibit KLF2 mRNA and protein expression by COMP-Angl; 2) AKT-CA induces the MEF2-dependent transcription and stimulates the KLF2 promoter cooperatively with MEF2; and 3) overexpression of AKT-CA induces both mRNA and protein expression of KLF2 in HUVECs. Currently, the reason for this discrepancy remains unclear, but it may be due to the different cell types used for the experiments. We performed the experiments with HUVECs, whereas they used an EOMA cell line. Alternatively, different stimuli such as Angl and shear stress may trigger distinct signaling pathways downstream of PI3K to stimulate KLF2 induction.

At present, a molecular link between AKT and MEF2 is still unknown. Recently, it has been reported that AKT directly phosphorylates transcriptional coactivator p300, leading to the association of MyoD with p300 and p300/CBP-associated factor (PCAF) (55). In addition, it has been also shown that p300 can physically interact with MEF2 as well as MyoD and enhances their transcriptional activity (28). Importantly, shear stress is shown to induce recruitment of p300 and PCAF into the KLF2 promoter (42). Therefore, the Angl/Tie2/PI3K/AKT pathway may induce the association of MEF2 with transcriptional coactivators such as p300 and PCAF, thereby stimulating its transcriptional activity. p300 directly acetylates and stimulates MEF2 activity (51). However, PI3K-mediated activation of MEF2 is not mediated by such direct acetylation mechanism because transcriptional activity of acetylation-defective mutant of MEF2 could be stimulated by constitutive active PI3K (supplemental Fig. S3). Thus, further examination is required for clarifying the molecular link between AKT and MEF2.

KLF2 inhibits VEGF-induced angiogenesis and inflammation, possibly by maintaining vascular quiescence. Similarly, Angl counteracts VEGF-mediated inflammatory responses. Our present data suggest that inhibition of VEGF-mediated inflammatory responses by Angl depends upon KLF2. However, Angl also acts cooperatively with VEGF to induce angiogenesis in a certain situation (5, 7, 9). This opposite effect of Angl on VEGF-mediated responses may depend upon whether KLF2 is induced or not. In the presence of cell-cell contacts, Angl/Tie2 signal is able to induce KLF2 expression and thereby inhibits VEGF-induced inflammation and angiogenesis. However, in the absence of cell-cell contacts, Angl/Tie2 signal accelerates angiogenic signal because KLF2 is not induced in this condition, which accounts for the cooperation of Angl with VEGF. Therefore, KLF2 may be a key downstream factor from *trans*-associated Tie2 to maintain vascular quiescence.

In conclusion, we found that Angl/Tie2 signal stimulates transcriptional activity of MEF2 through a PI3K/AKT pathway to induce KLF2 expression, thereby contributing to vascular quiescence.

Acknowledgments—We are grateful to M. K. Jain and G. B. Atkins (Case Western Reserve University) for the KLF2-Luc reporter plasmid, to Y. Fujio (Osaka University) for the adenovirus encoding AKT-CA, to C. Grozinger for the expression vector for HDAC5 (Harvard University), to K. Matsuo, M. Sone, M. Minamimoto, M. Maeoka, and Y. Matsuura for technical assistance, and to N. Takakura (Osaka University), M. Murakami (Kyoto University), H. Fujita (Osaka City University), and H. Daitoku (University of Tsukuba) for helpful advice.

REFERENCES

1. Dumont, D. J., Gradwohl, G., Fong, G. H., Puri, M. C., Gertsenstein, M., Auerbach, A., and Breitman, M. L. (1994) *Genes Dev.* **8,** 1897–1909
2. Suri, C., Jones, P. F., Patan, S., Bartunkova, S., Maisonpierre, P. C., Davis, S., Sato, T. N., and Yancopoulos, G. D. (1996) *Cell* **87,** 1171–1180
3. Sato, T. N., Tozawa, Y., Deutsch, U., Wolburg-Buchholz, K., Fujiwara, Y., Gendron-Maguire, M., Gridley, T., Wolburg, H., Risau, W., and Qin, Y. (1995) *Nature* **376,** 70–74
4. Wong, A. L., Haroon, Z. A., Werner, S., Dewhirst, M. W., Greenberg, C. S., and Peters, K. G. (1997) *Circ. Res.* **81,** 567–574
5. Peters, K. G., Kontos, C. D., Lin, P. C., Wong, A. L., Rao, P., Huang, L., Dewhirst, M. W., and Sankar, S. (2004) *Recent Prog. Horm. Res.* **59,** 51–71
6. Brindle, N. P., Saharinen, P., and Alitalo, K. (2006) *Circ. Res.* **98,** 1014–1023
7. Asahara, T., Chen, D., Takahashi, T., Fujikawa, K., Kearney, M., Magner, M., Yancopoulos, G. D., and Isner, J. M. (1998) *Circ. Res.* **83,** 233–240
8. Lin, P., Polverini, P., Dewhirst, M., Shan, S., Rao, P. S., and Peters, K. (1997) *J. Clin. Investig.* **100,** 2072–2078
9. Eklund, L., and Olsen, B. R. (2006) *Exp. Cell Res.* **312,** 630–641
10. Fukuhara, S., Sako, K., Minami, T., Noda, K., Kim, H. Z., Kodama, T., Shibuya, M., Takakura, N., Koh, G. Y., and Mochizuki, N. (2008) *Nat. Cell Biol.* **10,** 513–526
11. Saharinen, P., Eklund, L., Miettinen, J., Wirkkala, R., Anisimov, A., Winderlich, M., Nottebaum, A., Vestweber, D., Deutsch, U., Koh, G. Y., Olsen, B. R., and Alitalo, K. (2008) *Nat. Cell Biol.* **10,** 527–537
12. Kuo, C. T., Veselits, M. L., Barton, K. P., Lu, M. M., Clendenin, C., and Leiden, J. M. (1997) *Genes Dev.* **11,** 2996–3006
13. Lee, J. S., Yu, Q., Shin, J. T., Sebzda, E., Bertozzi, C., Chen, M., Mericko, P., Stadtfeld, M., Zhou, D., Cheng, L., Graf, T., MacRae, C. A., Lepore, J. J., Lo, C. W., and Kahn, M. L. (2006) *Dev. Cell* **11,** 845–857
14. Wu, J., Bohanan, C. S., Neumann, J. C., and Lingrel, J. B. (2008) *J. Biol. Chem.* **283,** 3942–3950
15. Atkins, G. B., and Jain, M. K. (2007) *Circ. Res.* **100,** 1686–1695
16. Dekker, R. J., van Soest, S., Fontijn, R. D., Salamanca, S., de Groot, P. G., VanBavel, E., Pannekoek, H., and Horrevoets, A. J. G. (2002) *Blood* **100,** 1689–1698
17. Huddleson, J. P., Srinivasan, S., Ahmad, N., and Lingrel, J. B. (2004) *Biol. Chem.* **385,** 723–729
18. Dekker, R. J., van Thienen, J. V., Rohlena, J., de Jager, S. C., Elderkamp, Y. W., Seppen, J., de Vries, C. J. M., Biessen, E. A. L., van Berkel, T. J. C., Pannekoek, H., and Horrevoets, A. J. G. (2005) *Am. J. Pathol.* **167,** 609–618
19. Parmar, K. M., Larman, H. B., Dai, G., Zhang, Y., Wang, E. T., Moorthy, S. N., Kratz, J. R., Lin, Z., Jain, M. K., Gimbrone, M. A., Jr., and Garcia-Cardena, G. (2006) *J. Clin. Investig.* **116,** 49–58
20. Kumar, A., Lin, Z., SenBanerjee, S., and Jain, M. K. (2005) *Mol. Cell. Biol.* **25,** 5893–5903
21. Hayashi, M., Kim, S. W., Imanaka-Yoshida, K., Yoshida, T., Abel, E. D., Eliceiri, B., Yang, Y., Ulevitch, R. J., and Lee, J. D. (2004) *J. Clin. Investig.* **113,** 1138–1148
22. Olson, E. N. (2004) *J. Clin. Investig.* **113,** 1110–1112
23. Wang, L., Fan, C., Topol, S. E., Topol, E. J., and Wang, Q. (2003) *Science* **302,** 1578–1581
24. SenBanerjee, S., Lin, Z., Atkins, G. B., Greif, D. M., Rao, R. M., Kumar, A., Feinberg, M. W., Chen, Z., Simon, D. I., Luscinskas, F. W., Michel, T. M., Gimbrone, M. A., Jr., Garcia-Cardena, G., and Jain, M. K. (2004) *J. Exp.*

Downloaded from www.jbc.org at National Cardiovascular Center, on April 25, 2010

Supplemental Material can be found at:
http://www.jbc.org/content/suppl/2008/12/23/M806928200.DC1.html
http://www.jbc.org/content/suppl/2009/02/19/284.9.5592.DC1.html

Med. **199,** 1305–1315
25. Lin, Z., Hamik, A., Jain, R., Kumar, A., and Jain, M. K. (2006) *Arterioscler. Thromb. Vasc. Biol.* **26,** 1185–1189
26. Bhattacharya, R., SenBanerjee, S., Lin, Z., Mir, S., Hamik, A., Wang, P., Mukherjee, P., Mukhopadhyay, D., and Jain, M. K. (2005) *J. Biol. Chem.* **280,** 28848–28851
27. Dekker, R. J., Boon, R. A., Rondaij, M. G., Kragt, A., Volger, O. L., Elderkamp, Y. W., Meijers, J. C. M., Voorberg, J., Pannekoek, H., and Horrevoets, A. J. G. (2006) *Blood* **107,** 4354–4363
28. Sartorelli, V., Huang, J., Hamamori, Y., and Kedes, L. (1997) *Mol. Cell. Biol.* **17,** 1010–1026
29. Gamble, J. R., Drew, J., Trezise, L., Underwood, A., Parsons, M., Kasminkas, L., Rudge, J., Yancopoulos, G., and Vadas, M. A. (2000) *Circ. Res.* **87,** 603–607
30. Kim, I., Moon, S. O., Hoon Kim, S., Jin Kim, H., Soon Koh, Y., and Young Koh, G. (2001) *J. Biol. Chem.* **276,** 7614–7620
31. Gavard, J., Patel, V., and Gutkind, J. S. (2008) *Dev. Cell* **14,** 25–36
32. Thurston, G., Suri, C., Smith, K., McClain, J., Sato, T. N., Yancopoulos, G. D., and McDonald, D. M. (1999) *Science* **286,** 2511–2514
33. Thurston, G., Rudge, J. S., Ioffe, E., Zhou, H., Ross, L., Croll, S. D., Glazer, N., Holash, J., McDonald, D. M., and Yancopoulos, G. D. (2000) *Nat. Med.* **6,** 460–463
34. Cho, C. H., Kammerer, R. A., Lee, H. J., Steinmetz, M. O., Ryu, Y. S., Lee, S. H., Yasunaga, K., Kim, K. T., Kim, I., Choi, H. H., Kim, W., Kim, S. H., Park, S. K., Lee, G. M., and Koh, G. Y. (2004) *Proc. Natl. Acad. Sci. U. S. A.* **101,** 5547–5552
35. Sakurai, A., Fukuhara, S., Yamagishi, A., Sako, K., Kamioka, Y., Masuda, M., Nakaoka, Y., and Mochizuki, N. (2006) *Mol. Biol. Cell* **17,** 966–976
36. Marinissen, M. J., Chiariello, M., Pallante, M., and Gutkind, J. S. (1999) *Mol. Cell. Biol.* **19,** 4289–4301
37. Coso, O. A., Montaner, S., Fromm, C., Lacal, J. C., Prywes, R., Teramoto, H., and Gutkind, J. S. (1997) *J. Biol. Chem.* **272,** 20691–20697
38. Murga, C., Fukuhara, S., and Gutkind, J. S. (2000) *J. Biol. Chem.* **275,** 12069–12073
39. Fukuhara, S., Sakurai, A., Sano, H., Yamagishi, A., Somekawa, S., Takakura, N., Saito, Y., Kangawa, K., and Mochizuki, N. (2005) *Mol. Cell. Biol.* **25,** 136–146
40. Fukuhara, S., Marinissen, M. J., Chiariello, M., and Gutkind, J. S. (2000) *J. Biol. Chem.* **275,** 21730–21736
41. Sen-Banerjee, S., Mir, S., Lin, Z., Hamik, A., Atkins, G. B., Das, H., Banerjee, P., Kumar, A., and Jain, M. K. (2005) *Circulation* **112,** 720–726
42. Huddleson, J. P., Ahmad, N., Srinivasan, S., and Lingrel, J. B. (2005) *J. Biol. Chem.* **280,** 23371–23379
43. Kato, Y., Kravchenko, V. V., Tapping, R. I., Han, J., Ulevitch, R. J., and Lee, J. D. (1997) *EMBO J.* **16,** 7054–7066
44. Kato, Y., Zhao, M., Morikawa, A., Sugiyama, T., Chakravortty, D., Koide, N., Yoshida, T., Tapping, R. I., Yang, Y., Yokochi, T., and Lee, J. D. (2000) *J. Biol. Chem.* **275,** 18534–18540
45. Sohn, S. J., Li, D., Lee, L. K., and Winoto, A. (2005) *Mol. Cell. Biol.* **25,** 8553–8566
46. McKinsey, T. A., Zhang, C. L., and Olson, E. N. (2002) *Curr. Opin. Cell Biol.* **14,** 763–772
47. McKinsey, T. A., Zhang, C. L., Lu, J., and Olson, E. N. (2000) *Nature* **408,** 106–111
48. Vega, R. B., Harrison, B. C., Meadows, E., Roberts, C. R., Papst, P. J., Olson, E. N., and McKinsey, T. A. (2004) *Mol. Cell. Biol.* **24,** 8374–8385
49. Potthoff, M. J., and Olson, E. N. (2007) *Development (Camb.)* **134,** 4131–4140
50. Han, J., Jiang, Y., Li, Z., Kravchenko, V. V., and Ulevitch, R. J. (1997) *Nature* **386,** 296–299
51. Ma, K., Chan, J. K. L., Zhu, G., and Wu, Z. (2005) *Mol. Cell. Biol.* **25,** 3575–3582
52. Bi, W., Drake, C. J., and Schwarz, J. J. (1999) *Dev. Biol.* **211,** 255–267
53. Deng, Y., Yang, J., McCarty, M., and Su, B. (2007) *Am. J. Physiol.* **293,** C1404–C1411
54. Xu, Q., and Wu, Z. (2000) *J. Biol. Chem.* **275,** 36750–36757
55. Serra, C., Palacios, D., Mozzetta, C., Forcales, S. V., Morantte, I., Ripani, M., Jones, D. R., Du, K., Jhala, U. S., Simone, C., and Puri, P. L. (2007) *Mol. Cell* **28,** 200–213

Downloaded from www.jbc.org at National Cardiovascular Center, on April 25, 2010

Provided for non-commercial research and education use.
Not for reproduction, distribution or commercial use.

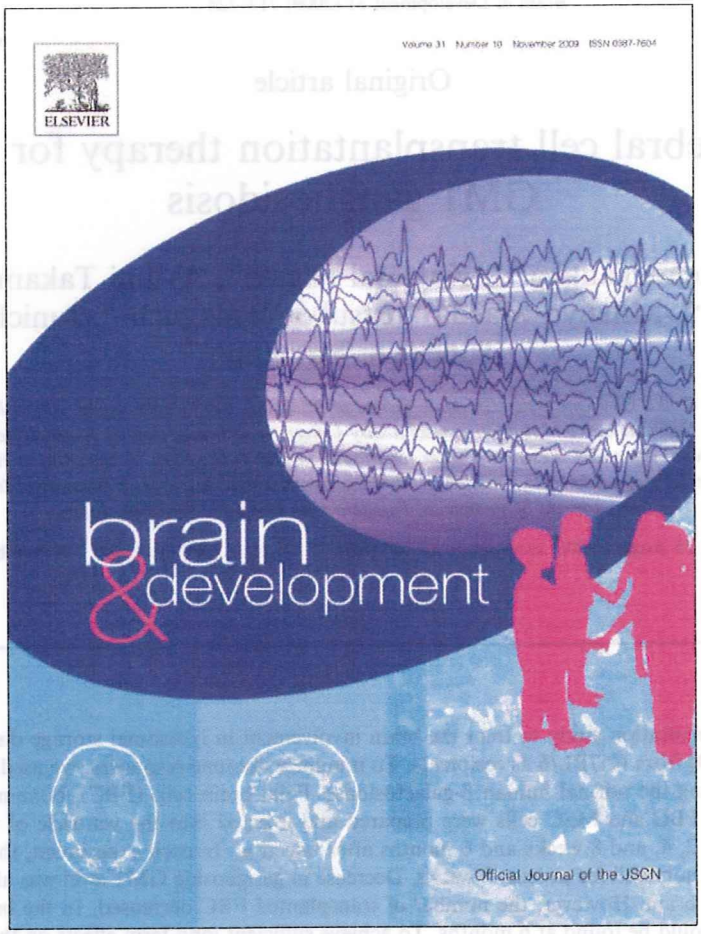

This article appeared in a journal published by Elsevier. The attached copy is furnished to the author for internal non-commercial research and education use, including for instruction at the authors institution and sharing with colleagues.

Other uses, including reproduction and distribution, or selling or licensing copies, or posting to personal, institutional or third party websites are prohibited.

In most cases authors are permitted to post their version of the article (e.g. in Word or Tex form) to their personal website or institutional repository. Authors requiring further information regarding Elsevier's archiving and manuscript policies are encouraged to visit:

http://www.elsevier.com/copyright

ELSEVIER

Brain & Development 31 (2009) 717–724

BRAIN & DEVELOPMENT
Official Journal of the Japanese Society of Child Neurology

www.elsevier.com/locate/braindev

Original article

Intracerebral cell transplantation therapy for murine GM1 gangliosidosis

Tomo Sawada [a], Akemi Tanaka [a,*], Katsumi Higaki [c], Ayumi Takamura [c], Eiji Nanba [c], Toshiyuki Seto [a,e], Mitsuyo Maeda [b], Etsuko Yamaguchi [a], Junichiro Matsuda [d], Tunekazu Yamano [a]

[a] *Department of Pediatrics, Osaka City University Graduate School of Medicine, 1-4-3 Asahi-machi, Abeno-ku, Osaka 545-8585, Japan*
[b] *Department of Neurobiology and Anatomy, Osaka City University Graduate School of Medicine, Osaka, Japan*
[c] *Division of Functional Genomics, Research Center for Bioscience and Technology, Tottori University, Yonago, Japan*
[d] *Laboratory of Experimental Animal Models, Division of Bioresources, National Institute of Biomedical Innovation, Osaka, Japan*
[e] *Department of Pediatrics, Fujiidera City Hospital, Fujiidera, Japan*

Received 25 August 2008; received in revised form 15 October 2008; accepted 1 November 2008

Abstract

We performed a cell transplantation study to treat the brain involvement in lysosomal storage diseases. We used acid β-galactosidase knock-out mice (BKO) from C57BL/6 as recipients. To minimize immune responses, we used cells derived from transgenic mice of C57BL/6 overexpressing the normal human β-galactosidase. Fetal brain cells (FBC), bone marrow-derived mesenchymal stem cells (MSC), and mixed FBC and MSC cells were prepared and injected into the ventricle of newborn BKO mouse brain. The mice were examined at 1, 2, 4, and 8 weeks and 6 months after injection. In each experiment, the injected cells migrated into the whole brain effectively and survived for at least 8 weeks. Decrease in ganglioside GM1 level was also observed. FBC could survive for 6 months in recipient brain. However, the number of transplanted FBC decreased. In the brains of MSC- or mixed cell-treated mice, no grafted cells could be found at 6 months. To achieve sufficient long-term effects on the brain, a method of steering the immune response away from cytotoxic responses or of inducing tolerance to the products of therapeutic genes must be developed.
© 2008 Elsevier B.V. All rights reserved.

Keywords: GM1-gangliosidosis; Cell transplantation; Fetal brain cell; Mesenchymal stem cell

1. Introduction

Enzyme replacement therapy (ERT), hematopoeitic stem cell transplantation (HSCT), and gene transfer have been studied in animals and in humans with lysosomal storage disease (LSD). ERT is now available clinically for Gaucher disease, Fabry disease, Pompe disease, and MPS I, II, and VI in many countries, and has been successful in visceral organs. HSCT is also effective against the somatic involvements in Gaucher disease and MPS I, II, and VI. However, HSCT exhibits little efficacy in conditions such as Fabry disease and Pompe disease, when enzyme secretion from donor cells is poor or the uptake of enzyme proteins by the affected host cells is inadequate. In addition, efficacy in individual organs differs markedly, in both ERT and HSCT, depending on accessibility of blood flow and the density of mannose-6-phosphate receptors. Neither HSCT nor ERT exhibits efficacy against the brain involvement in Gaucher or MPSs because of the poor access due to the blood–brain barrier.

Many experimental studies have been carried out, involving methods such as gene therapy [1–5], cell

* Corresponding author. Tel.: +81 6 6645 3816; fax: +81 6 6636 8737.
E-mail address: akemi-chan@med.osaka-cu.ac.jp (A. Tanaka).

0387-7604/$ - see front matter © 2008 Elsevier B.V. All rights reserved.
doi:10.1016/j.braindev.2008.11.004

therapy [6–9], or intrathecal administration of enzymes [10,11], for treatment of the brain in LSDs. Such treatments were able to overcome the blood–brain barrier to access brain tissue and exhibit considerable efficacy in brain. However, it is difficult to maintain such efficacy for long periods of time. Repetition of these treatments is not practical because intracranial administration is required for them. On the other hand, the usefulness of intravenous administration is limited because of the blood–brain barrier, except in newborn mice which have an immature barrier. It has been reported that intravenous administration of extremely high doses of enzymes [12–14] or of enzymes that remain in the circulation for long periods [15,16] yielded slight passage through the blood–brain barrier, though with increase in the risk of immune response.

Oral administration of small molecules would be a good and convenient method of treatment of the brain for prolonged periods, such as substrate reduction therapy with *N*-butyldeoxynojirimycin or *N*-butyldeoxygalactonojirimycin for glycosphingolipidoses [17–19] or genistein for mucopolysaccharidoses [20], and chemical chaperone therapy for Fabry disease [21] or GM1-gangliosidosis [22]. However, the efficacy of substrate reduction therapies has thus far been quite limited, and chemical chaperone therapies are not applicable for every type of gene mutation.

GM1 gangliosidosis is an LSD and a progressive neurological disease in humans caused by a genetic defect of lysosomal acid β-galactosidase, which hydrolyses the terminal β-galactosidic residue of ganglioside GM1 and other glycoconjugates. The defects in β-galactosidase activity result in accumulation of ganglioside GM1 in various organs, especially the brain, causing progressive neurodegeneration. In our previous study [2], we injected recombinant adenovirus encoding mouse β-galactosidase cDNA intravenously in β-galactosidase-deficient newborn mice, and showed that vector-mediated β-galactosidase-producing brain cells could reduce ganglioside GM1 accumulation. We showed that β-galactosidase enzyme protein could be secreted as well as taken up by the brain cells and function effectively. However, the efficacy obtained was transient. If sufficient amounts of the defective enzyme could be permanently secreted by cells in the brain, injury of the brain could be prevented. To examine the possibility of long-term cell treatment of the brain in LSDs, we carried out a transplantation experiment in the brain of a GM1-gangliosidosis mouse model (acid β-galactosidase knock-out mouse) using fetal brain cells (FBC) and mesenchymal stem cells (MSC) from bone marrow. These cells used for transplantation were derived from mice of the same genetic background as recipient mice except for possession of the human β-galactosidase gene.

2. Materials and methods

2.1. Knock-out and transgenic mice

A mouse model of GM1 gangliosidosis (BKO mouse) was generated by targeting of the β-galactosidase gene at exon 15 in ES cells as previously described [23]. Newborn mice were obtained by mating heterozygous female mice with homozygous male mice. Identification of newborn mutants was accomplished by quantitative analysis of β-galactosidase activity in tail tip homogenates on the day of birth. Mice with high β-galactosidase activity (TG mice) [24] were generated by introducing the human β-galactosidase gene as a transgene in ES cells obtained from the BKO mouse, which has several copies of the human β-galactosidase gene without the mouse β-galactosidase background. Age-matched wild-type mice of C57BL/6 strain were used as a control.

2.2. Cell preparations for transplantation

Cultured mesenchymal stem cells (MSC) were obtained from the bone marrow of the tibias and femurs of 5–8 month-old TG mice according to the method of Meirelles et al. [25] with some modifications. Dulbecco's modified Eagle's medium (DMEM: Sigma Chemical Co., St Louis, MO) containing 10% fetal bovine serum (Medical and Biological Laboratories, Nagoya, Japan) was used for culture.

Fetal brain cells (FBC) were obtained from the fetal cerebral cortex of TG mice at 13 days of gestation according to the method of Meberg and Miller [26]. The brain tissue was disrupted in a Pasteur glass pipette by gentle stroking several times (uncultured FBC), and then cultured for 4 h in Neurobasal medium (Invitrogen, Carlsbad, CA, No. 12348-07) containing 2 mM glutamine and 10% FBS, followed by two days in Neurobasal medium containing 2 mM glutamine and B27 supplement (Invitrogen, No. 14175-095) (cultured FBC).

2.3. Transplantation of cells into newborn mouse brain

Each BKO mouse received a single injection of 0.5–1.0×10^5 of the cells prepared as described above in the right cerebral ventricle from 24 to 48 hours after birth. Study groups were as follows: uncultured FBC ($n = 18$), cultured FBC ($n = 10$), MSC ($n = 17$), and mixed MSC and FBC (1:1) ($n = 15$). Mice of each experimental group were divided into three subgroups for X-gal staining, β-galactosidase assay and ganglioside GM1 analysis. Mice were examined at one, two, four, and eight weeks and 6 months after injection as shown in Table 1.

For biochemical analysis, mice were anesthetized with diethylether and the blood was washed out with normal saline by perfusion through the heart, and the

brains were removed and kept at −80 °C until use. For histological studies, the brains were fixed by perfusion through the heart with 4% paraformaldehyde in 0.1 M phosphate buffer pH 7.4 (PB) for 20 min., after washing out the blood with normal saline. To obtain frozen sections, the brains were placed in 0.1 M phosphate buffer pH 7.4 containing 30% sucrose, and frozen in liquid nitrogen.

All surgical and care procedures were carried out in accordance with the Guidelines for Use and Care of Experimental Animals approved by the Animal Committee of Osaka City University School of Medicine.

2.4. X-Gal staining

Frozen sections (16 μm thick) were reacted with X-gal using the β-gal staining Kit (Invitrogen Corp., Carlsbad, CA) to visualize β-galactosidase activity.

2.5. β-Galactosidase assay

β-Galactosidase activity was analyzed in the tissue homogenate with the artificial substrate 2 mM 4-methylumbelliferyl β-galactoside at pH 4.0 in 0.1 M sodium citrate-phosphate buffer according to the method described by Suzuki [27]. Protein was analyzed using the Bio-Rad protein assay system (Bio-Rad Laboratories, Hercules, CA) with the method of Bradford [28].

2.6. Analysis of ganglioside GM1

Amounts of ganglioside GM1 were measured by immunoblot assay using anti-GM1 ganglioside monoclonal antibody (Code: 370685, Seikagaku Corp., Tokyo, Japan) by the method of Michikawa et al. [29] with some modifications.

Brain tissue cells were disrupted by sonication and solubilized in 20 mM Tris–HCl buffer pH 8.0 containing 137 mM NaCl, 10% glycerol, and a protease inhibitor cocktail (Complete, Mini, Cat No. 11836153001, Roche Diagnostics, Mannheim, Germany). Five micrograms of tissue protein was applied onto Trans-Blot Transfer Medium Pure Nitrocellulose Membrane (0.45 μm pore size, Code: 162-0117, Bio-Rad Laboratories) through the slots of a Bio-Dot SF Microfiltration Apparatus (Bio-Rad Laboratories). The membrane was reacted with anti-GM1 ganglioside monoclonal antibody diluted 1:500, after blocking with 5% skim milk in PBS solution for 1 h at room temperature, and then with horseradish peroxidase-linked anti-mouse IgG sheep antibody (Code: NA931, GE Healthcare UK Ltd., Buckinghamshire, UK) diluted 1:1,000. The washing solution used was 0.1 M Tris buffered saline pH 7.5 containing 0.1% Tween 20 (TTBS). Bound antibody was detected using ECL after reaction with ECL™ Western Blotting Detection Reagents (Code: RPN2209, GE Healthcare UK Ltd.) and visualized on X-ray film. Densitometric quantification of immunoreactive signal was performed using the Kodak Digital Science™ EDAS 120 system with 1D Image Analysis software (Eastman Kodak Company, NY). The values obtained were compared with those of quantification of histological immunoreactivity with Leica Control Software as previously described [30], and the same ratios were obtained among the samples (data not shown). The assay was performed three times and in duplicate for each sample independently, and mean values were calculated.

3. Results

3.1. X-Gal staining

Layered staining of the transplanted cells was observed over the entire ventricular surface on both sides of the cerebral hemispheres in treated mice at one week after injection (data not shown). Positive cells had spread into the brain tissue by two weeks (Fig. 1c and f) in the mice treated with cultured FBC ($n = 1$), uncultured FBC ($n = 1$), and MSC ($n = 2$) in the same amounts. The cells had spread further and had reached every part of the brain by 4 weeks in the mice of all experimental groups (Fig. 1d, g and i). Less positive cells were found in the mice treated with MSC ($n = 3$) or mixed MSC and FBC ($n = 3$) (Fig. 1g and i) than in the mice treated with cultured ($n = 3$) or uncultured FBC ($n = 3$) (Fig. 1d). The number of the X-Gal positive cells increased gradually until 4 weeks after injection in every experimental mouse. At 8 weeks after injection, positive cells still existed in the cultured FBC- ($n = 3$) and uncultured FBC-treated ($n = 3$) mice (Fig. 1e) in the same numbers with a similar distribution as at 4 weeks. However, a significant decrease in number of positive cells was found at 8 weeks in the mice treated with MSC ($n = 3$) or mixed MSC and FBC ($n = 3$) (Fig. 1h and j). In the mice treated with mixed MSC and FBC, positive cells existed in higher numbers in deep areas than in the mice treated with MSC alone. In the mice treated with cultured ($n = 2$) and uncultured FBC ($n = 2$), small numbers of positive cells with strong staining still existed in many parts of the brain, especially around the striatum and lateral globs pallidus (Fig. 1k and l), at 6 months after injection. No grafted cells were found in the mice treated with MSC ($n = 1$) or mixed MSC and FBC ($n = 1$) at 6 months. No significant differences were noted among the mice within each experimental group at each stage.

3.2. β-Galactosidase activity

The β-galactosidase activity in FBC and MSC derived from TG mice were 214.5–227.5 nmol/mg/h ($n = 4$) and 143.0–121.4 nmol/mg/h ($n = 3$), respec-

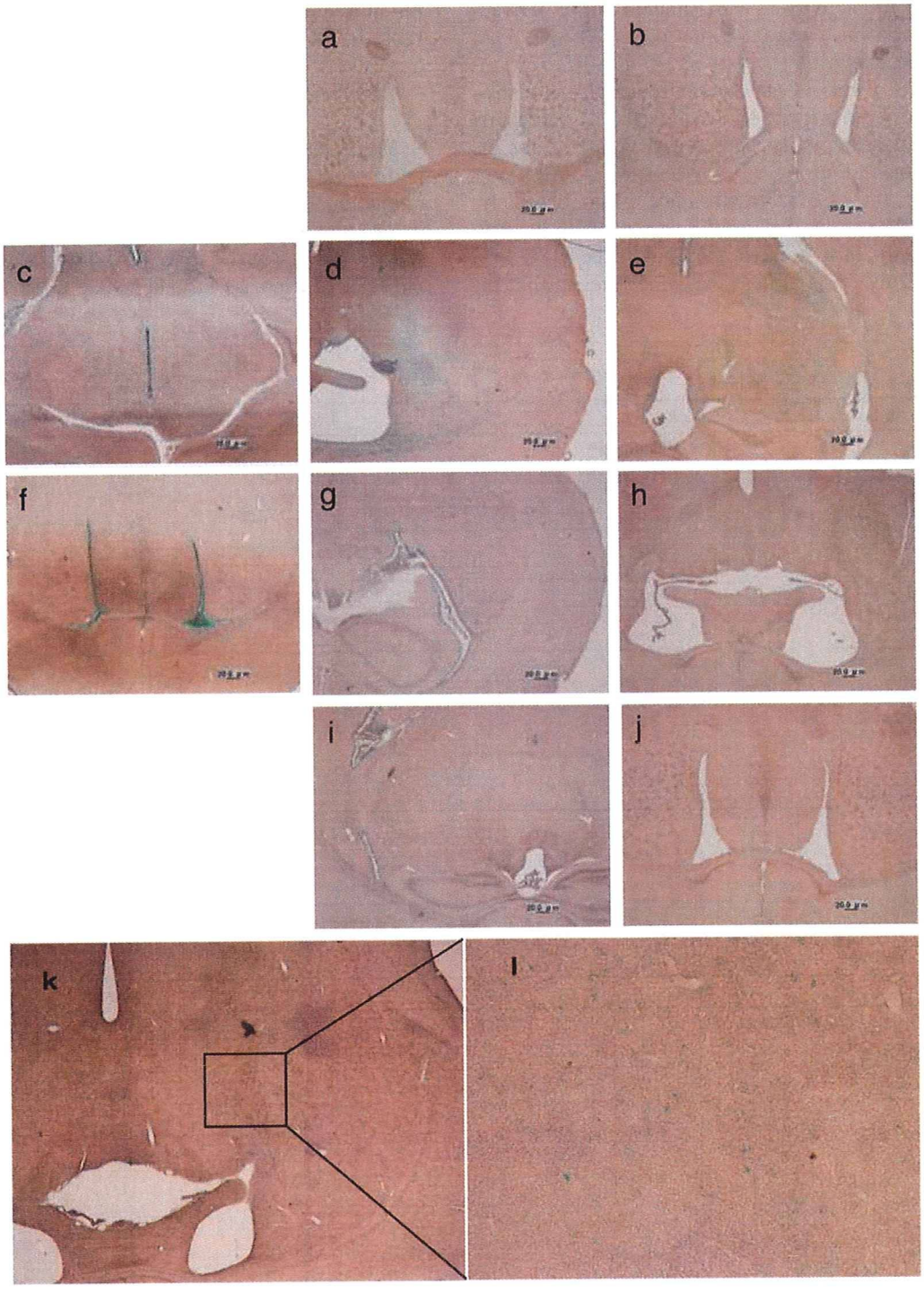

Fig. 1. X-Gal staining of brain coronal sections at +0.8 mm to −2.0 mm of bregma. (a and b) Non-treated BKO mouse at 4 and 8 weeks old, respectively; (c–e) Treated with FBC at 2, 4, and 8 weeks after injection; (f–h) Treated with MSC at 2, 4, and 8 weeks after injection; (i and j) Treated with mixed MSC and FBC at 4 and 8 weeks after injection; (k) FBC-treated brain at 6 months after injection; (l) Magnification of figure k. Positive cells had spread into the brain tissue by two weeks (c and f). The cells had spread further by 4 weeks (d, g and i). Less positive cells were found in the mice treated with MSC or mixed MSC and FBC (g and i) than in the mice treated with FBC (d). At 8 weeks, positive cells still existed in FBC-treated mouse (e) as at 4 weeks (d). A significant decrease in number of positive cells was found at 8 weeks in the mice treated with MSC (h) or mixed MSC and FBC (j). Strong positive staining cells still existed at 6 months in the brain of FBC-treated mouse (k and l).

tively, while the activity in FBC and in MSC derived from wild-type mice were 54.9–69.1 ($n = 2$) and 63.0 ($n = 1$), respectively.

The results of brain β-galactosidase activity in transplantation experiments are shown in Table 2. Increases in β-galactosidase activity were found in the brains of each experimental group at 4 weeks after injection. Activity in the FBC-treated mice was definitely increased at 4 weeks as well as at 8 weeks, while activity at 8 weeks in the MSC-treated mice and mixed MSC and FBC-treated mice was almost the same level as that in the untreated mice. These findings were consistent with those in the X-Gal staining study.

3.3. Immunoassay of ganglioside GM1

Immunoassay of accumulated ganglioside GM1 was performed for each mouse using anti-GM1 ganglioside monoclonal antibody. Values are ratios to the amounts in age-matched normal control mice. The results are shown in Fig. 2 and Tables 3. At 4 weeks after injection, remarkable decrease in ganglioside GM1 accumulation

Table 1
Mouse numbers used for each experiment.

Time after injection	1 week	2 weeks	4 weeks	8 weeks	6 months
	[X-Gal staining]				
Uncultured FBC	1	1	3	3	2
Cultured FBC	1	1	3	3	2
MSC		2	3	3	1
Mixed MSC and FBC			3	3	1
	[β-galactosidase activity]				
Uncultured FBC			2	2	
Cultured FBC					
MSC			2	2	
Mixed MSC and FBC			2	2	
	[Immunoblot assay of ganglioside GM1 amount]				
Uncultured FBC			1	1	1
Cultured FBC					
MSC			2	2	
Mixed MSC and FBC			2	2	

Table 2
β-Galactosidase activity.

	4 weeks	8 weeks
Age-matched normal control (mean ± SD)	197 ± 61 ($n = 7$)	159 ± 56 ($n = 7$)
Non-treated (mean ± SD)	4.38 ± 0.35 ($n = 5$)	4.10 ± 0.47 ($n = 5$)
Treated with uncultured FBC	Mouse 1	Mouse 7
	Rt: 6.65[a]	Rt: 4.94
	Lt: 5.31[a]	Lt: 6.03[a]
	Mouse 2	Mouse 8
	Rt: 7.36[a]	Rt: 5.58[a]
	Lt: 5.33[a]	Lt: 5.05[a]
Treated with MSC	Mouse 3	Mouse 9
	Rt: 6.30[a]	Rt: 4.13
	Lt: 5.95[a]	Lt: 3.67
	Mouse 4	Mouse 10
	Rt: 5.74[a]	Rt: 4.19
	Lt: 5.12[a]	Lt: 5.05[a]
Treated with mixed MSC and FBC	Mouse 5	Mouse 11
	Rt: 5.80[a]	4.13 (mix of both hemispheres)
	Lt: 5.40[a]	
	Mouse 6	Mouse 12
	Rt: 5.06	Rt: 4.85
	Lt: 4.52	Lt: 5.02

Values are in nmol/mg/h. Each sample was tested in duplicate and results are mean values. Rt, right hemisphere; Lt, left hemisphere.
[a] Increase of activity over mean + 2SD of non-treated mice.

Table 3
Immunoblot assay of ganglioside GM1 amount.

	4 weeks	8 weeks	6 months
Age-matched non-treated (range)	2.65–3.55 ($n = 3$)	4.98–5.28 ($n = 3$)	7.58 (n = 1)
Treated with uncultured FBC	Mouse I	Mouse VI	Mouse XI
	Rt: 1.42[a]	Rt: 2.30[a]	Rt: 6.18[b]
	Lt: 1.80[a]	Lt: 2.44[a]	Lt: 6.40[b]
Treated with MSC	Mouse II	Mouse VII	
	Rt: 1.82[a]	Rt: 5.30	
	Lt: 1.31[a]	Lt: 5.23	
	Mouse III	Mouse VIII	
	Rt: 1.40[a]	Rt: 4.40[b]	
	Lt: 1.34[a]	Lt: 4.73[b]	
Treated with mixed MSC and FBC	Mouse IV	Mouse IX	
	Rt: 1.33[a]	Rt: 4.55[b]	
	Lt: 1.34[a]	Lt: 4.78[b]	
	Mouse V	Mouse X	
	Rt: 1.78[a]	Rt: 4.45[b]	
	Lt: 1.62[a]	Lt: 4.58[b]	

Values are ratios to those for age-matched control mice. Each sample was tested in duplicate for three times and results are mean values. Rt, right hemisphere; Lt, left hemisphere.
[a] Remarkable decrease.
[b] Slight decrease of ganglioside GM1 compared with non-treated mice.

was found in the mice of every group. However, at 8 weeks, decrease was detected only in the mouse treated with FBC. Efficacy was still noted at 6 months after injection in FBC-treated mouse. These findings were consistent with those for X-Gal staining (Fig. 1) and β-galactosidase activity (Table 2).

4. Discussion

Two therapeutic methods, HSCT and ERT, are clinically available for LSDs. However, neither is markedly effective in the brain. A number of experiments in animal models have been carried out on the treatment of brain in LSDs. Each revealed some efficacy in the brain, though it was transient and incomplete. Sufficient enzyme expression throughout life is needed in the brain. Thus, permanent engraftment of enzyme-secreting cells in the brain, or permanent expression of an exogenous gene with a vector or as an integrated gene might eliminate the brain involvement in LSDs.

However, the immune responses of host animals are among the most difficult problems to overcome in this respect [31–33]. Although the brain, which is sequestered from systemic immune responses, is thought to exhibit little immune response, elimination of cells expressing a therapeutic transgene occurs in the brain. We speculate that innate inflammatory immune responses are stimulated to kill such cells, not necessarily with the induction of a linked adaptive immune response. When host brain cells express a therapeutic transgene mediated by a viral vector, the host cells themselves will be eliminated, possibly resulting in acceleration of neuronal cell death in neurodegenerative disorders. Transplantation of cells having the same genetic information as the host animals with LSD except for expression of a deficient enzyme protein would thus be a good method of treatment for avoiding the elimination of host neuronal cells and curing diseased host cells.

We performed cell transplantation into the brain of β-galactosidase-deficient mice to study the usefulness of long-term engraftment for supplementation of deficient enzyme protein. To minimize the immune responses in the recipient β-galactosidase knock-out mice, we used cells of mice with the same genetic background as the recipient except for possession of copies of the human β-galactosidase gene.

Initially, in the transplantation experiment, we used FBC from transgenic mice expressing the human β-galactosidase gene. The cells could grow in an environment similar to that of the recipient organ in which they were originally growing. The cells spread into the brains and the cell number increased at least until 4 weeks. They grew very successfully for at least 8 weeks and survived for 6 months or more. However, the number of engrafted cells had decreased significantly at 6 months, while the size of the brain had increased. The decrease in ganglioside GM1 accumulation was also marked until 8 weeks after transplantation. However, at 6 months, this decrease was far less pronounced, with re-accumulation of ganglioside GM1. After the cells were engrafted and the cell number was increased by the cell division in the recipient brain, they were depleted. The mechanism of depletion of transplanted cells involved immunological rejection, although the transplanted cells were very similar genetically and physiologically to the recipient.

Next, we performed a transplantation experiment using MSCs obtained from the bone marrow of the

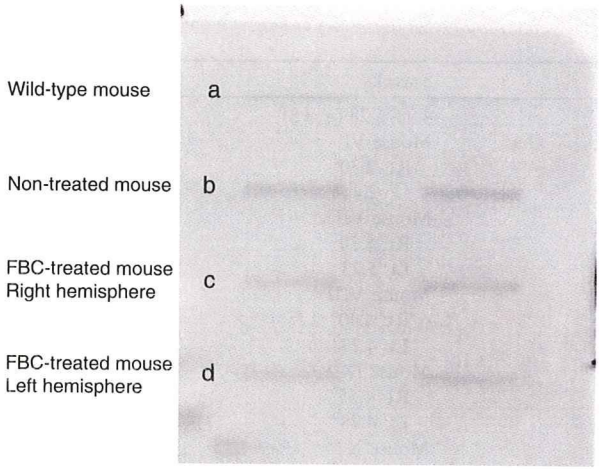

Fig. 2. Immunoblot assay of ganglioside GM1 in brain homogenate at 8 weeks after treatment. Performed in duplicate as shown in two slots for each sample. (a) Wild-type mouse; (b) Non-treated mouse; (c and d) Right and left hemisphere, respectively, of a mouse treated with FBC. The immunoreactivity against ganglioside GM1 antibody in the treated brain (c and d) was less than non-treated brain (d). The accumulated amounts of ganglioside GM1 were calculated in the ratio to the age-matched wild-type mouse (a) from the densitometric quantification signals. These values were shown in Table 3.

same mice expressing the human β-galactosidase gene. MSCs were obtained using the method of plastic adherence. This relatively crude procedure produces a heterogeneous population including multipotential MSCs. These crude cells were used to avoid depletion of potentially important cells and for ease of preparation for clinical application. The cells spread into the brains and the cell number increased similarly to FBC transplantation experiment until 4 weeks. However, decrease in number of engrafted living cells and efficacy in preventing accumulation of ganglioside GM1 were observed in the examination of 8-week-old treated mice.

A number of studies on neural transdifferentiation have been reported [34–37]. Some have reported that neural transdifferentiation of MSCs is induced by cell fusion with host neuronal cells [38–41]. We therefore used mixed FBC and MSC cells to stimulate cell fusion. More engrafted cells were found in the deep areas of the mouse brains treated with mixed cells than in the brains treated with MSC alone. However, no fused cells could be identified. The long-living cells were probably transplanted FBC themselves.

Decrease of ganglioside GM1 was observed even though the increase of the β-galactosidase activity was so small. Similar efficacy was shown previously in our gene therapy experiment [2]. On the other hand, we observed a general depletion of the transplanted cells over time in the BKO mouse brains. The transplanted cells survived in early stage and the number increased by cell division, then, died. This was likely caused by immunological rejection, even though we used fetal brain cells (FBC) from mice with the same genetic background for transplantation. We speculated that immunological reaction occurred because these cells expressed the therapeutic enzyme protein which the host animals did not have. The same has been reported in the transplantation of autogenous cells expressing an exogenous therapeutic gene [33]. The grafted cells were gradually depleted because of immunological rejection by the host animals. To avoid deleterious immune attack and to achieve sufficient long-term efficacy in brain, development of methods to steer the immune response away from cytotoxic responses or to induce tolerance to the products of therapeutic genes is needed [42,43].

Acknowledgements

We thank Kaoru Takano and Takanori Kunieda for mating of mice and providing the BKO and TG mice in timely fashion for each experiment.

This work was supported by grant AT-18591163 from the Ministry of Education, Culture, Sports, Science, and Technology of Japan.

References

[1] Shen JS, Watabe K, Ohashi T, Eto Y. Intraventricular administration of recombinant adenovirus to neonatal twitcher mouse leads to clinicopathological improvements. Gene Ther 2001;8:1081–7.

[2] Takaura N, Yagi T, Maeda M, Nanba E, Oshima A, Suzuki Y, et al. Attenuation of ganglioside GM1 accumulation in the brain of GM1 gangliosidosis mice by neonatal intravenous gene transfer. Gene Ther 2003;10:1487–93.

[3] Kim EY, Hong YB, Lai Z, Cho YH, Brady RO, Jung SC. Long-term expression of the human glucocerebrosidase gene in vivo after transplantation of bone-marrow-derived cells transformed with a lentivirus vector. J Gene Med 2005;7:878–87.

[4] Shen JS, Meng XL, Yokoo T, Sakurai K, Watabe K, Ohashi T, et al. Widespread and highly persistent gene transfer to the CNS by retrovirus vector in utero: implication for gene therapy to Krabbe disease. J Gene Med 2005;7:540–51.

[5] Cachón-González MB, Wang SZ, Lynch A, Ziegler R, Cheng SH, Cox TM. Effective gene therapy in an authentic model of Tay-Sachs-related diseases. Proc Natl Acad Sci USA 2006;103:10373–8.

[6] Kopen GC, Prockop DJ, Phinney DG. Marrow stromal cells migrate throughout forebrain and cerebellum, and they differentiate into astrocytes after injection into neonatal mouse brains. Proc Natl Acad Sci USA 1999;96:10711–6.

[7] Jin HK, Carter JE, Huntley GW, Schuchman EH. Intracerebral transplantation of mesenchymal stem cells into acid sphingomyelinase-deficient mice delays the onset of neurological abnormalities and extends their life span. J Clin Invest 2002;109:1183–91.

[8] Sakurai K, Iizuka S, Shen JS, Meng XL, Mori T, Umezawa A, et al. Brain transplantation of genetically modified bone marrow stromal cells corrects CNS pathology and cognitive function in MPS VII mice. Gene Ther 2004;11:1475–81.

[9] Givogri MI, Galbiati F, Fasano S, Amadio S, Perani L, Superchi D, et al. Oligodendroglial progenitor cell therapy limits central

neurological deficits in mice with metachromatic leukodystrophy. J Neurosci 2006;26:3109–19.
[10] Kakkis E, McEntee M, Vogler C, Le S, Levy B, Belichenko P, et al. Intrathecal enzyme replacement therapy reduces lysosomal storage in the brain and meninges of the canine model of MPS I. Mol Genet Metab 2004;83:163–74.
[11] Dickson P, McEntee M, Vogler C, Le S, Levy B, Peinovich M, et al. Intrathecal enzyme replacement therapy: successful treatment of brain disease via the cerebrospinal fluid. Mol Genet Metab 2007;91:61–8.
[12] Vogler C, Levy B, Grubb JH, Galvin N, Tan Y, Kakkis E, et al. Overcoming the blood–brain barrier with high-dose enzyme replacement therapy in murine mucopolysaccharidosis VII. Proc Natl Acad Sci USA 2005;102:14777–82.
[13] Matzner U, Herbst E, Hedayati KK, Lüllmann-Rauch R, Wessig C, Schröder S, et al. Enzyme replacement improves nervous system pathology and function in a mouse model for metachromatic leukodystrophy. Hum Mol Genet 2005;14:1139–52.
[14] Blanz J, Stroobants S, Lüllmann-Rauch R, Morelle W, Lüdemann M, D'Hooge R, et al. Reversal of peripheral and central neural storage and ataxia after recombinant enzyme replacement therapy in {alpha}-mannosidosis mice. Hum Mol Genet 2008;17:3437–45.
[15] Grubb JH, Vogler C, Levy B, Galvin N, Tan Y, Sly WS. Chemically modified {beta}-glucuronidase crosses blood–brain barrier and clears neuronal storage in murine mucopolysaccharidosis VII. Proc Natl Acad Sci USA 2008;105:2616–21.
[16] Montaño AM, Oikawa H, Tomatsu S, Nishioka T, Vogler C, Gutierrez MA, et al. Acidic amino acid tag enhances response to enzyme replacement in mucopolysaccharidosis type VII mice. Mol Genet Metab 2008;94:178–89.
[17] Kasperzyk JL, El-Abbadi MM, Hauser EC, D'Azzo A, Platt FM, Seyfried TN. *N*-butyldeoxygalactonojirimycin reduces neonatal brain ganglioside content in a mouse model of GM1 gangliosidosis. J Neurochem 2004;89:645–53.
[18] Lachmann RH, te Vruchte D, Lloyd-Evans E, Reinkensmeier G, Sillence DJ, Fernandez-Guillen L, et al. Treatment with miglustat reverses the lipid-trafficking defect in Niemann-Pick disease type C. Neurobiol Dis 2004;16:654–8.
[19] Cox TM. Substrate reduction therapy for lysosomal storage diseases. Acta Paediatr Suppl. 2005;94:69–75.
[20] Piotrowska E, Jakóbkiewicz-Banecka J, Barańska S, Tylki-Szymańska A, Czartoryska B, Wegrzyn A, et al. Genistein-mediated inhibition of glycosaminoglycan synthesis as a basis for gene expression-targeted isoflavone therapy for mucopolysaccharidoses. Eur J Hum Genet 2006;14:846–52.
[21] Ishii S, Yoshioka H, Mannen K, Kulkarni AB, Fan JQ. Transgenic mouse expressing human mutant alpha-galactosidase A in an endogenous enzyme deficient background: a biochemical animal model for studying active-site specific chaperone therapy for Fabry disease. Biochim Biophys Acta 2004;1690:250–7.
[22] Matsuda J, Suzuki O, Oshima A, Yamamoto Y, Noguchi A, Takimoto K, et al. Chemical chaperone therapy for brain pathology in G(M1)-gangliosidosis. Proc Natl Acad Sci USA 2003;100:15912–7.
[23] Matsuda J, Suzuki O, Oshima A, Ogura A, Noguchi Y, Yamamoto Y, et al. Beta-galactosidase-deficient mouse as an animal model for GM1-gangliosidosis. Glycoconj J 1997;14:729–36.
[24] Yamamoto Y, Nagase Y, Noguchi A, Mochida K, Nakahira M, Takano K, et al. Generation and characterization of the β-galactosidase knockout mouse having the normal human β-galactosidase gene as a transgene (in Japanese). Proc Jap Soc of Animal Models for Hum Dis (Nippon Shikkan Model Gakkai Kiroku) 2001;17:20–2.
[25] Meirelles Lda S, Nardi NB. Murine marrow-derived mesenchymal stem cell: isolation, in vitro expansion, and characterization. Br J Haematol 2003;123:702–11.
[26] Meberg PJ, Miller MW. Culturing hippocampal and cortical neurons. Methods Cell Biol 2003;71:111–27.
[27] Suzuki K. Enzymatic diagnosis of sphingolipidosis. Methods Enzymol 1987;138:727–62.
[28] Bradford MM. A Rapid and sensitive method for the quantitation of microgram quantities of protein utilizing the principle of protein-dye binding. Anal Biochem 1976;72:255–60.
[29] Michikawa M, Gong JS, Fan QW, Sawamura N, Yanagisawa K. A novel action of alzheimer's amyloid beta-protein (Abeta): oligomeric Abeta promotes lipid release. J Neurosci 2001;21:7226–35.
[30] Suzuki Y, Ichinomiya S, Kurosawa M, Ohkubo M, Watanabe H, Iwasaki H, et al. Chemical chaperone therapy: clinical effect in murine G(M1)-gangliosidosis. Ann Neurol 2007;62:671–5.
[31] Barker RA, Widner H. Immune problems in central nervous system cell therapy. NeuroRx 2004;1:472–81.
[32] Abordo-Adesida E, Follenzi A, Barcia C, Sciascia S, Castro MG, Naldini L, et al. Stability of lentiviral vector-mediated transgene expression in the brain in the presence of systemic antivector immune responses. Hum Gene Ther 2005;16:741–51.
[33] Lowenstein PR, Kroeger K, Castro MG. Immunology of neurological gene therapy: how T cells modulate viral vector-mediated therapeutic transgene expression through immunological synapses. Neurotherapeutics 2007;4:715–24.
[34] Weimann JM, Charlton CA, Brazelton TR, Hackman RC, Blau HM. Contribution of transplanted bone marrow cells to Purkinje neurons in human adult brains. Proc Natl Acad Sci USA 2003;100:2088–93.
[35] Abouelfetouh A, Kondoh T, Ehara K, Kohmura E. Morphological differentiation of bone marrow stromal cells into neuron-like cells after co-culture with hippocampal slice. Brain Res 2004;1029:114–9.
[36] Wislet-Gendebien S, Hans G, Leprince P, Rigo JM, Moonen G, Rogister B. Plasticity of cultured mesenchymal stem cells: switch from nestin-positive to excitable neuron-like phenotype. Stem cells 2005;23:392–402.
[37] Deng J, Petersen BE, Steindler DA, Jorgensen ML, Laywell ED. Mesenchymal stem cells spontaneously express neural proteins in culture and are neurogenic after transplantation. Stem cells 2006;24:105410–64.
[38] Terada N, Hamazaki T, Oka M, Hoki M, Mastalerz DM, Nakano Y, et al. Bone marrow cells adopt the phenotype of other cells by spontaneous cell fusion. Nature 2002;416:542–5.
[39] Alvarez-Dolado M, Pardal R, Garcia-Verdugo JM, Fike JR, Lee HO, Pfeffer K, et al. Fusion of bone-marrow-derived cells with Purkinje neurons, cardiomyocytes and hepatocytes. Nature 2003;425:968–73.
[40] Kozorovitskiy Y, Gould E. Stem cell fusion in the brain. Nat Cell Biol 2003;5:952–4.
[41] Bae JS, Furuya S, Shinoda Y, Endo S, Schuchman EH, Hirabayashi Y, et al. Neurodegeneration augments the ability of bone marrow-derived mesenchymal stem cells to fuse with Purkinje neurons in Niemann-Pick type C mice. Hum Gene Ther 2005;16:1006–11.
[42] Tomatsu S, Gutierrez M, Nishioka T, Yamada M, Yamada M, Tosaka Y, et al. Development of MPS IVA mouse (Galnstm(hC79S. mC76S)slu) tolerant to human *N*-acetylgalactosamine-6-sulfate sulfatase. Hum Mol Genet 2005;14:3321–5.
[43] Matzner U, Matthes F, Herbst E, Lüllmann-Rauch R, Callaerts-Vegh Z, D'Hooge R, et al. Induction of tolerance to human arylsulfatase A in a mouse model of metachromatic leukodystrophy. Mol Med 2007;13:471–9.

Developmental Biology 331 (2009) 140–151

Contents lists available at ScienceDirect

Developmental Biology

journal homepage: www.elsevier.com/developmentalbiology

The transcriptional repressor RP58 is crucial for cell-division patterning and neuronal survival in the developing cortex

Haruo Okado [a,*,1,2,3], Chiaki Ohtaka-Maruyama [a,1,2,4], Yoshinobu Sugitani [b,1,2,4], Yuko Fukuda [c,2], Reiko Ishida [c,2], Shinobu Hirai [a,2], Akiko Miwa [a,2], Akiyo Takahashi [a,2], Katsunori Aoki [d,2], Keiji Mochida [e,2,4], Osamu Suzuki [f,4], Takao Honda [g,2], Kazunori Nakajima [g,4], Masaharu Ogawa [b,4], Toshio Terashima [h,4], Junichiro Matsuda [f,2,5], Hitoshi Kawano [i,1,4], Masataka Kasai [c,1]

[a] *Department of Molecular Physiology, Tokyo Metropolitan Institute for Neuroscience, 2-6 Musashidai, Fuchu, Tokyo 183-8526, Japan*
[b] *Ogawa research unit, Neuro-developmental disorder research group, Brain Science Institute, Riken, Saitama 351-0198, Japan*
[c] *Department of Immunology, National Institute of Infectious Diseases, 1-23-1 Toyama, Shinjuku-ku, Tokyo 162-8640, Japan*
[d] *Department of Hematology (Internal Medicine), The University of Tokyo, Bunkyo-ku, Tokyo 113-8655, Japan*
[e] *Bioresource Center, RIKEN, Tsukuba, Ibaraki 305-0074, Japan*
[f] *Department of Veterinary Science, National Institute of Infectious Diseases, 1-23-1 Toyama, Shinjuku-ku, Tokyo 162-8640, Japan*
[g] *Department of Anatomy, Keio University School of Medicine, Tokyo 160-8582, Japan*
[h] *Division of Anatomy and Developmental Neurobiology, Department of Neuroscience, Kobe University Graduate School of Medicine, Kobe 650-0017, Japan*
[i] *Department of Developmental Morphology, Tokyo Metropolitan Institute for Neuroscience, 2-6 Musashidai, Fuchu, Tokyo 183-8526, Japan*

ARTICLE INFO

Article history:
Received for publication 23 August 2008
Revised 1 April 2009
Accepted 24 April 2009
Available online 3 May 2009

Keywords:
RP58
Transcriptional repressor
Cerebral cortex
Apoptosis
Cell-cycle exit
Progenitor cell

ABSTRACT

The neocortex and the hippocampus comprise several specific layers containing distinct neurons that originate from progenitors at specific development times, under the control of an adequate cell-division patterning mechanism. Although many molecules are known to regulate this cell-division patterning process, its details are not well understood. Here, we show that, in the developing cerebral cortex, the RP58 transcription repressor protein was expressed both in postmitotic glutamatergic projection neurons and in their progenitor cells, but not in GABAergic interneurons. Targeted deletion of the *RP58* gene led to dysplasia of the neocortex and of the hippocampus, reduction of the number of mature cortical neurons, and defects of laminar organization, which reflect abnormal neuronal migration within the cortical plate. We demonstrate an impairment of the cell-division patterning during the late embryonic stage and an enhancement of apoptosis of the postmitotic neurons in the *RP58*-deficient cortex. These results suggest that RP58 controls cell division of progenitor cells and regulates the survival of postmitotic cortical neurons.
© 2009 Elsevier Inc. All rights reserved.

Introduction

Glutamatergic cortical neurons are generated from progenitor cells in the cortical germinal zone and migrate radially in an inside-to-outside gradient. The earliest neurons form the preplate (together with the Cajal-Retzius cells) and the neurons born subsequently migrate past the earliest-born neurons to intercalate within the preplate, divide it into the marginal zone (MZ; layer 1) and the subplate (layer 6b), and form the lower layers of the cortical plate (CP). Late-born neurons then migrate past the early-born neurons to form the upper layers of the CP, beneath the MZ. In contrast, GABAergic neurons and Cajal-Retzius cells are generated from progenitor cells outside the neocortex, in the ganglion eminence and in the cortical hem, respectively, and migrate tangentially into the neocortex (Bayer and Altman, 1991; Allendoerfer and Shatz, 1994; Molyneaux et al., 2007). The radial glial progenitors (RGPs) in the ventricular zone (VZ) give rise to cortical neurons, while the progenitor cells in the subventricular zone (SVZ) produce a substantial number of upper-layer neurons (Smart and McSherry, 1982, Tarabykin et al., 2001, Sugitani et al., 2002). Some of the SVZ progenitor cells are intermediate progenitors (IMPs), which originate from the VZ and produce neurons by dividing limited times (Noctor et al., 2004; Haubensak et al., 2004; Miyata et al., 2004). In the hippocampus, pyramidal neurons of the Cornu Ammonis (CA) are generated from the VZ of the hippocampus, whereas the precursors of the granular neurons of the dentate gyrus (DG) originate in the neuroepithelium near the cortical hem, migrate towards the anlage of

* Corresponding author.
E-mail address: hokado@tmin.ac.jp (H. Okado).
[1] H.O, C.O-M, Y.S, H.K. and M.K. designed the research.
[2] H.O, C.O-M, Y.S., Y.F., R.I., S.H., A.M., A.T., K.A., K.M., T.H., J.M. performed the research.
[3] H.O. wrote the paper.
[4] C.O-M, Y.S., O.S., K.N., M.O. T.T., H.K., K.M. provided helpful discussion and guidance.
[5] Present address: National Institute of Biomedical Innovation, Ibaraki City, Osaka 567-0085, Japan.

0012-1606/$ – see front matter © 2009 Elsevier Inc. All rights reserved.
doi:10.1016/j.ydbio.2009.04.030

the DG, continue to divide, and undergo further migration to the granule layer of the DG (Forster et al., 2006; Li and Pleasure 2007).

These cortical progenitor cells generate a vast diversity of terminally differentiated neuronal phenotypes. The balance between exit from and reentry into the cell cycle is important for the formation of these cell types at appropriate times; however, the molecular mechanism underlying this regulation is not completely understood (Dehay and Kennedy, 2007).

We have previously described a novel DNA binding protein, RP58 (also known as ZNF238), which shares homology with the POZ domain of a number of zinc finger (ZF) proteins, which are termed POZ-ZF proteins (Aoki et al., 1998). RP58 exhibits a sequence-specific transcriptional repressor activity (Aoki et al., 1998) and probably acts by binding to the DNA methyltransferase Dnmt3a, which associates with histone deacetylase and acts as a corepressor (Fuks et al., 2001). POZ-ZFs are important for many biological processes, which include B-cell fate determination, DNA damage responses, cell-cycle progression, and a multitude of developmental events (Kelly and Daniel, 2006). Among the POZ-ZF proteins, the promyelocytic leukemia zinc finger (PLZF) is essential for stem cell self renewal in the murine testis (Buaas et al., 2004; Costoya et al. 2004), Miz1 plays an essential role in the control of the exit from the cell cycle during the hair cycle (Gebhardt et al., 2007), and ZENON is involved in the maintenance of panneuronal features and/or in the survival of mature neurons (Kiefer et al., 2005).

We demonstrated that RP58 transcripts are highly expressed in the cerebral cortex in the embryonic mouse brain (Ohtaka-Maruyama et al., 2007). In addition, RP58 is expressed weakly in the VZ and intensely in the SVZ, intermediate zone (IZ), and CP in the embryonic cortex, which suggests that RP58 is important for the early development of cortical neurons. In adult cerebral cortex, the expression of the RP58 transcript is maintained in glutamatergic neurons, but not in GABAergic neurons.

In the present study, we investigated the role of RP58 in the development of the cerebral cortex by generating and analyzing *RP58*-deficient mice. Our results demonstrate that *RP58* deficiency causes enhanced apoptosis and impairs the cell-division patterning in the VZ during late development, which suggests that RP58 is a novel regulator of glutamatergic neuron survival and of progenitor cell division.

Materials and methods

Generation of RP58-deficient mice

Similarly to what is observed for the human *RP58* gene, the sequence of the mouse *RP58* gene that encodes the functional protein is uninterrupted over its entire 4.2 kb length (Meng et al., 2000). A gene-targeting construct was prepared by deletion of the entire exon (5.4 kb). The resulting *RP58* targeting vector (Supplementary Fig. 1A), which was constructed from a mouse strain 129 library (Stratagene) and consisted of a 4.2 kb homology arm derived from the 5' end of the exon, a PGK promoter-neomycin expression cassette, and a 2.7 kb homology arm from the 3' end of the exon, was linearized with XbaI and introduced into GSI ES cells (derived from the 129/SvJ mouse strain) by electroporation. Colonies that survived after selection were picked and expanded for DNA analysis. Targeted ES cells were injected into the blastocoel cavity of C57/BL6 embryos using a piezo-driven micromanipulator (PrimeTech, Tsuchiura, Japan) to generate chimeric mice, which were then crossed with C57/BL6 females to obtain heterozygous $RP58^{+/-}$ mutant animals. These mice were, in turn, interbred to produce homozygous $RP58^{-/-}$ mice at the expected Mendelian frequency.

Southern blot analysis of genomic DNA isolated from the tails of embryonic day (E) 18.5 fetuses confirmed the homologous integration of the target vector (Supplementary Fig. 1B), which resulted in the replacement of the entire *RP58* exon (5.4 kb) with the neomycin resistance gene. Northern blot analysis of total RNA extracted from genotyped embryonic brains (Supplementary Fig. 1C) showed that the RP58 transcript was present only in wild-type and heterozygous embryos. In homozygous mutant embryos, no RP58 transcript of any size was observed. Embryonic brain extracts were incubated with anti-RP58-conjugated Sepharose 4B beads. The beads were washed extensively and boiled in SDS sample buffer. After centrifugation, the supernatant was analyzed for the presence of RP58 by immunoblotting, as described previously (Ishida et al., 2002). To confirm the specificity of the interactions between the antigen and the antibody, the peptide (CLPTVRDWTLEDSSQELWK) used for the generation of the anti-RP58 antibody was added during the immunoprecipitation experiment. Antibodies specific to RP58 detected the protein in brain extracts from wild-type, but not homozygous mutant, embryos (Supplementary Fig. 1D). The day after the mating was designated E0.5.

Immunohistochemistry

Heads of embryos were removed, fixed in Bodian's fixative (3.7% formaldehyde, 80% ethanol), embedded in paraffin, and sectioned at an 8 μm thickness. A few embryos were perfused with 4% paraformaldehyde and sectioned using a cryostat (10–25 μm thickness). In most cases, the antigens in these sections were reactivated by heating in 10 mM citrate buffer (adjusted to pH 6.0) using a microwave or an autoclave.

We used the following antibodies: rabbit anti-mouse RP58 (1:500, Takahashi et al., 2008), mouse anti-reelin (1:200, Chemicon), rabbit anti-MAP2 (1:500, Chemicon), rabbit anti-Tbr1 (1:500, Chemicon), rabbit anti-Prox1 (1:1000, Covance), chicken anti-Tuj1 (1:200, Chemicon), mouse anti-BrdU (1:50, Becton-Dickinson), rat anti-BrdU (1:200, Abcam), mouse anti-α-synuclein, mouse anti-β-synuclein (1:200, BD Transduction Lab), rabbit anti-Pax6 (1:200, Chemicon), mouse anti-PCNA (1:200, Chemicon), mouse anti-nestin (1:200, Rat-401), mouse anti-NeuN (1:100, Chemicon), mouse anti-Ki67 (1:100, Novocastra), rabbit anti-Ki67 (1:500, Novocastra), goat anti-NeuroD (1:100, Santa Cruz Biotechnology), guinea pig anti-Dlx2 (1:1000, gift from Dr. Yoshikawa; Kuwajima et al., 2006), mouse anti-Neurogenin2 (1:5, gift from Dr. Anderson), rabbit anti-phosphohistone H3 (P-H3) (1: 200, Upstate), rabbit anti-neurofilament (1:500, Fukuda et al., 1997), rabbit anti-ssDNA (1:400, DAKO), rabbit anti-active caspase 3 (1:400, R&D), and goat anti-Unc5d (1:200, R&D).

Anti-IgG antibodies conjugated to biotin (Vector, 1:200), Alexa 488, Alexa 546, Alexa 555, Cy3, or Cy5 (1:500) (Molecular Probes or Jackson Laboratories) were used as secondary antibodies and the ABC kit (Vector) or the TSA Fluorescence System (PerkinElmer) were used to detect biotin. After nuclear staining with DAPI and Topro3, the sections were mounted with PermaFluor (Immunon) or were dehydrated and mounted with Entellan Neu (Merk). A laser-scanning confocal microscope was used to image fluorescence signals.

To perform RP58/Pax6 and RP58/Tbr2 double labeling using rabbit polyclonal antibodies, we used the TSA or TSA Plus Fluorescence System (PerkinElmer), according to Friocourt et al. (2008). Sections were first incubated with diluted anti-RP58 antibody (1:8000), for the TSA Plus Fluorescence System, and were then incubated with rabbit anti-Pax6 antibody (1:200), anti-Tbr2 antibody (1:200), or no antibody (negative control). For RP58/P-H3 double labeling, sections were first incubated with anti-RP58 antibody (1:500), for the TSA Fluorescence System, and were then incubated with rabbit anti-P-H3 antibody (1:200). For Pax6/Tbr2 double labeling, sections were first incubated with diluted anti-Pax6 antibody (1:30000), for the TSA Plus Fluorescence System, and were then incubated with rabbit anti-Tbr2 antibody (1:200). For Pax6/Tbr2/Unc6d triple labeling, sections were first incubated with diluted anti-Pax6 antibody (1:15000), for the TSA Plus Fluorescence System, and were then incubated with rabbit anti-Tbr2 (1:200) and anti-Uncd5 (1:200) antibodies.

RNA in situ hybridization

We used single-stranded digoxigenin (DIG)-UTP-labeled RNA probes generated from the mouse *RP58* cDNA (approximately 1.6 kb); mouse *ER81* (a gift from Dr. Jessell; Arber et al., 2003); mouse *RORβ* (a gift from Dr. McConnell; Weimann et al., 1999); *Svet1* (a gift from Dr. Tarabykin; Tarabykin et al., 2001); *NT3* (a gift from Dr. Aizawa; Shinozaki et al., 2004); rat *SCIP* (a gift from Dr. Lemke), mouse α-crystalline (a gift from Dr. Funatsu; Funatsu et al., 2004), rat *KA1* (a gift from Dr. Boulter; Better et al., 1990), for mouse *Tbr1*, mouse *mSorLA*; mouse *CTGF*, and mouse *Tailless* (gifts from Drs. Y Sugitani and T Noda; Sugitani et al., 2002); *HES5* cDNA (a gift from Dr. Guillemot; Cau et al., 2000). Some probes were hydrolyzed to a length of about 200–500 bp. RNA *in situ* hybridization was performed on Bodian's-fixed paraffin sections, according to the method of Ohtaka-Maruyama et al. (2007), and on 4% paraformaldehyde-fixed frozen sections, according to the method of Sugitani et al. (2002). In some cases, the counterstaining was performed using Nuclear Fast Red (Kernechtrot).

BrdU- and IdU-labeling experiments

Bromodeoxyuridine (BrdU) or iododeoxyuridine (IdU) (50 mg/kg of body weight) were injected intraperitoneally into pregnant mice at various developmental stages. To estimate the rates of cell-cycle exit, randomly selected BrdU-positive cells (about 50 cells) were examined for PCNA or Pax6 immunoreactivity 24 h after the incorporation of BrdU. In particular, the rates of cell-cycle exit were estimated in the lower region (which corresponded to the VZ) and in the upper region (which corresponded to the SVZ and IZ) of E16.5 embryos in which BrdU was incorporated on E15.5. The total number of BrdU-positive cells was counted and examined for Pax6 immunoreactivity (which corresponds to 0.09 mm of the ventricular surface). The SVZ was identified by staining with Unc5d/Svet1.

To estimate the production of progenitor cells, randomly selected Ki67-positive cells were examined for BrdU immunoreactivity 0.5 h after the incorporation of BrdU.

The estimation of cell-cycle kinetics was performed according to Martynoga et al. (2005). P_{cells} was estimated by counting the total number of cells in the prospective VZ within the sampling area.

TUNEL assay

Apoptosis was detected using a TUNEL assay kit (Dead End Fluorometric TUNEL system, Promega). Deparaffinized sections were treated with proteinase K (20 μg/ml) in 100 mM Tris–Cl and 50 mM EDTA (pH = 8.0) for 15 min at room temperature (RT), followed by treatment with FITC-nucleotide containing TdT or H_2O (as a negative control), and counterstaining using propidium iodide.

Results

Targeted disruption of the RP58 gene

To study the role of RP58 in the development of the central nervous system, we disrupted the *RP58* gene in embryonic stem cells using the target vector (see Supplementary Fig. 1A and "Materials and methods" section). Heterozygous ($RP58^{+/-}$) mice were phenotypically indistinguishable from their wild-type littermates, whereas all homozygous ($RP58^{-/-}$) mice, which were generated from intercrosses of the heterozygotes, died shortly after birth. The cause of the death remains unknown and is currently under investigation.

Hypoplasia of the hippocampus and neocortex in RP58-deficient mice

Because RP58 transcripts are expressed abundantly in the brain of the wild-type mice ($RP58^{+/+}$; Ohtaka-Maruyama et al., 2007) and $RP58^{-/-}$ mice die shortly after birth, we performed histological analyses of brains isolated from null, heterozygous, and wild-type animals at neonatal and embryonic stages. We observed hypoplasia of the neocortex and hippocampus in $RP58^{-/-}$ mice, whereas the brains of $RP58^{+/-}$ mice appeared to be normal (Fig. 1; Supplementary Figs. 1E–M). Therefore, we compared $RP58^{-/-}$ mice with either wild-type or $RP58^{+/-}$ mice in subsequent experiments. The neocortex of $RP58^{-/-}$ mice displayed a reduced thickness and its layers were disorganized. Furthermore, the VZ appeared to expand radially in the mutant cortex (asterisk in Fig. 1). In the mutant hippocampus, the pyramidal cell layer and the typical V-shaped granule cell layer of the DG were not evident (Fig. 1). Additionally, the cerebellum of $RP58^{-/-}$ mice lacked the typical foliation observed in wild-type and heterozygous animals (see Supplementary Figs. 1K–M). In the present study, we focused our analysis on the neocortex and hippocampus of mutant mice.

Reduced numbers of mature neurons in the mutant neocortex and hippocampus

Double staining of the neocortex with MAP2 and β-III-Tubulin (Tuj1) showed that postmitotic neurons were present in the mutant neocortex; however, the subplate layer was incompletely formed in the medial region of the mutant neocortex (arrowheads in Supplementary Figs. 2A–B").

To further characterize this abnormality of the neocortex, we examined the expression of various layer markers. The number of E19 subplate neurons positive for the connective tissue growth factor (CTGF), which labels maturing subplate neurons in layer 6b (Friedrichsen et al., 2003; Heuer et al., 2003), was drastically decreased in the mutant neocortex when compared with the wild type (Figs. 2A and B). To detect the subplate neurons at the earlier stage, we examined the staining for β-synuclein, which is an inhibitor

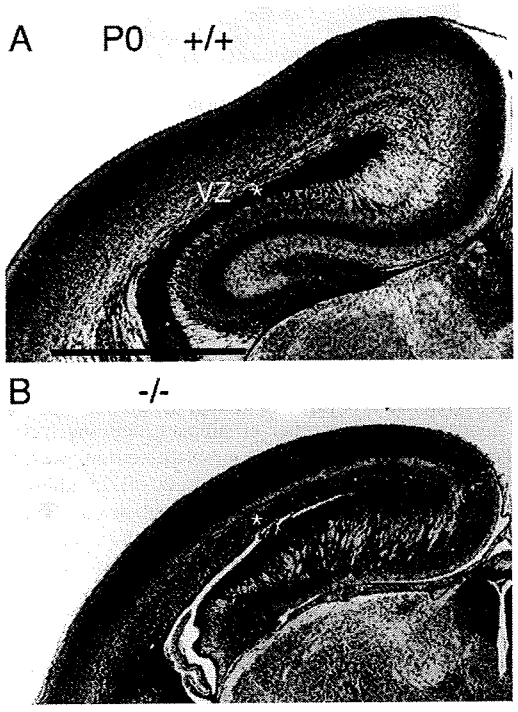

Fig. 1. Defects in brain formation in $RP58^{-/-}$ mice at P0. Nissl-stained coronal sections of forebrains from (A) wild-type (+/+) and (B) *RP58*-deficient (−/−) mice showed cytoarchitectural abnormalities in the neocortex and hippocampus of the mutant animal. In the mutant, the thickness of the neocortex was reduced and the ventricular zone (VZ) (marked with an asterisk) was expanded. Cresyl violet staining. Scale bar, 1 mm (A, B).

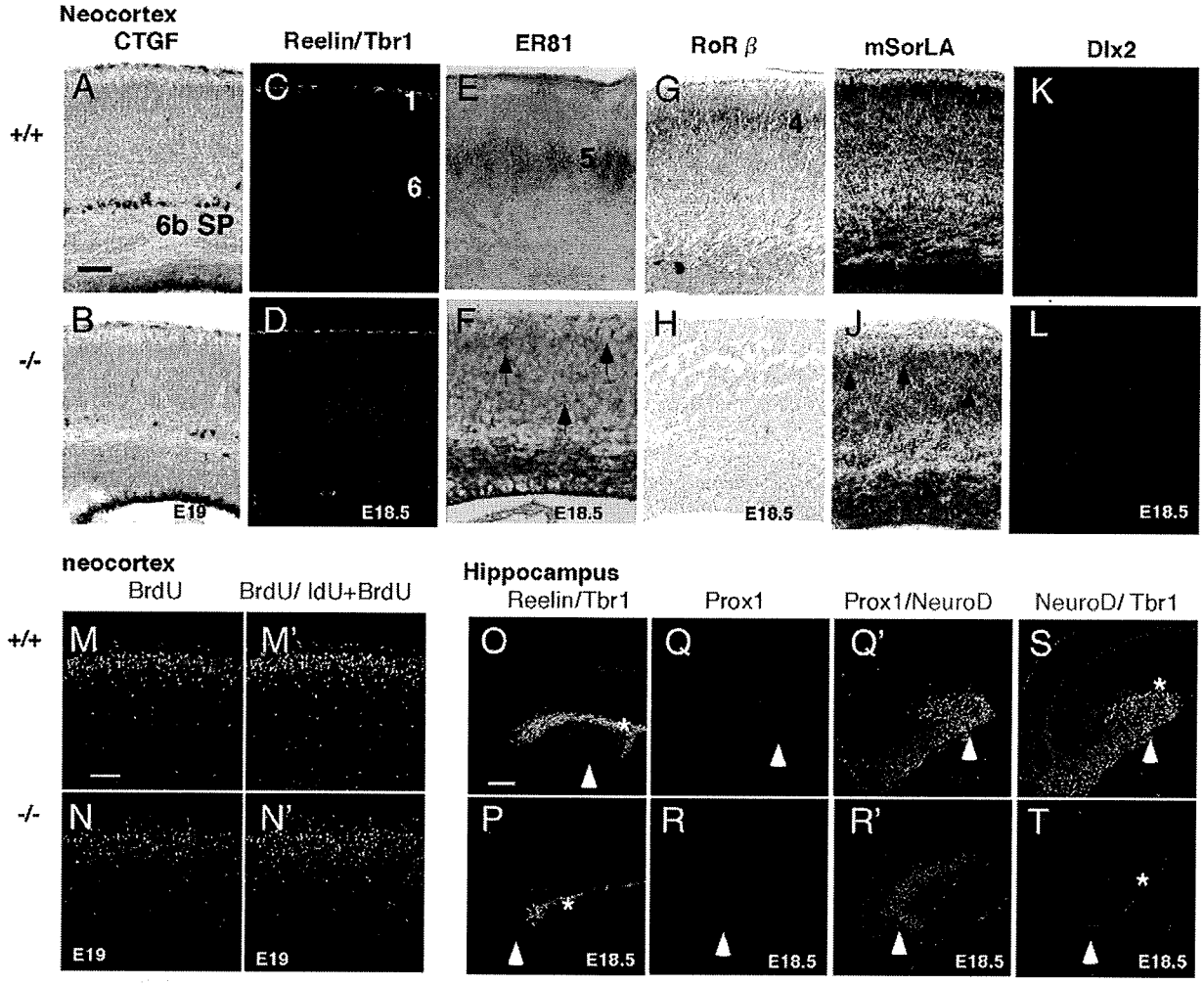

Fig. 2. Dysplasia of the neocortex and hippocampus in *RP58*$^{-/-}$ mice. (A–L) The disorganized laminar structures of the neocortex and hippocampus of the mutant were demonstrated by various layer-specific markers at E19 (A and B) or E18.5 (C–L) in the wild-type (+/+) and *RP58*-deficient (−/−) neocortex. (A and B) CTGF-labeled subplate neurons, (C and D) reelin-labeled layer 1 Cajal-Retzius neurons and Tbr1-labeled layer 6 cortical neurons, (E and F) ER81-labeled layer 5 cortical neurons, (G and H) *RoR*β-labeled layer 4 cortical neurons, (I and J) mSorLA-labeled layer 2/3 cortical neurons, and (K and L) Dlx2-labeled GABAergic neurons. In the mutant neocortex, the subplate neurons were sharply reduced in number (A and B), Cajal-Retzius neurons were normal (C and D), Tbr1-positive cells were shifted more superficially and were more widely scattered when compared with the wild type (C and D), ER81- and mSorLA-positive cells were located diffusely and in reduced numbers (arrows in F and J), the expression level of *RoR*β was dramatically reduced (G and H), and Dlx1-positive cells were roughly normal (K and L). Scale bar, 0.1 mm (A–L).

of the aggregation of α-synuclein (Hashimoto et al. 2001), as a marker for subplate neurons. Since β-synuclein is mostly detected in the deepest region of layer 6, identified with Tbr1 immunoreactivity, β-synuclein-positive cells correspond to the subplate neurons in the wild-type cortex at E16.5 (arrows in Supplementary Figs. 2E–E"). In mutant neocortices, the number of subplate neurons was severely reduced and a part of the surviving subplate neurons was displaced superficially at E16.5 (Supplementary Figs. 2C–F). In addition, in the *RP58* mutants, a fraction of the neurofilament-positive thalamocortical fibers (Kawano et al., 1999), which use subplate neurons for their pathfinding, abnormally projected towards the surface of the neocortex (Fig. 3).

Reelin-positive Cajal-Retzius neurons (Ogawa et al., 1995) developed normally in layer 1 in the E18.5 mutant (Figs. 2C and D, green). In the E18.5 mutant cortex, the majority of the Tbr1-positive cells was located in the deeper part of cortical plate (Fig. 2C; Supplementary Fig. 4E); however, many of these cells were also detected diffusely throughout the CP (Fig. 2D; Supplementary Fig. 3F). ER81, which is a layer 5 marker (Sugitani et al., 2002), was expressed in many cells in the wild-type CP (Fig. 2E); in contrast, this marker was expressed in only a few cells in the E18.5 mutant CP (arrows in Fig. 2F). Cells in the mutant cortex were only faint positive for *ROR*β, which labels layer 4 neurons (Weimann et al., 1999) (Figs. 2G and H). mSorLA labels layer 2/3 neurons (Fig. 2I, Sugitani et al., 2002; Hermans-Borgmeyer et al., 1998); mSorLA-positive cells in the mutant cortex were diffusely distributed and dramatically reduced in number (arrows in Fig. 2J). In contrast, GABA-positive (data not shown) and Dlx2-positive (Figs. 2K and L) inhibitory interneurons of the mutant neocortex did not display any distinct abnormalities, although their distribution pattern appeared slightly disturbed. These results suggest that mature subplate neurons and mature CP neurons, which form the future cortical layers 2–5, were reduced in number in *RP58*$^{-/-}$ mice.

The diffuse distribution of Tbr1-positive and other cortical neurons in the mutant cortex raised the possibility that the *RP58* deficiency impaired the inside-out layer formation. To examine this possibility, we performed double labeling by injecting iododeoxyuridine (IdU) at E12.5 and 5-bromo-2-deoxyuridine (BrdU) at E14.5, followed by examination of the brains at E19 (Figs. 2M–N'). Most late-born cortical neurons (Figs. 2M' and N', yellow) crossed over early-born cells (Figs. 2M' and N', red) in the wild-type cortex, while many late-born neurons were abnormally located beneath early-born cells in the mutant cortex. The defects of laminar organization observed in the

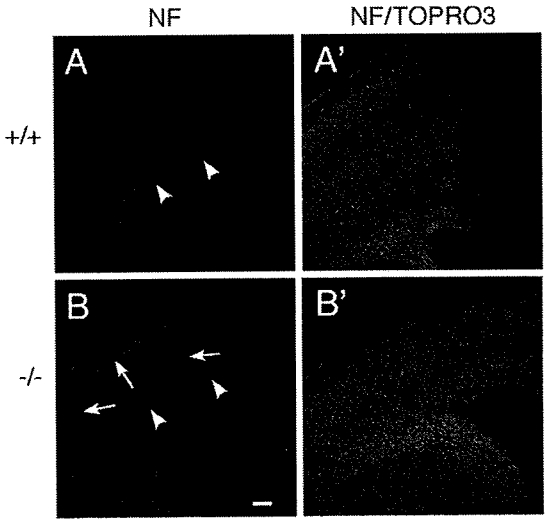

Fig. 3. Abnormality of the thalamocortical pathway formation in the *RP58*-deficent cortex. Coronal sections from E18.5 wild-type (A, A') and *RP58*$^{-/-}$ (B, B') brains stained with anti-neurofilament (NF) antibodies and TOPRO3 (nuclear stain) (A', B'). In the wild type, thalamocortical axons that were immunoreactive for neurofilament ran along the subplate beneath the cortical plate (arrowheads in A), while in the *RP58*$^{-/-}$ brain, some labeled axons ran along the subplate beneath the cortical plate (arrowheads in B), whereas the other axons invaded the cortical plate towards the pial surface (arrows in B). Scale bar, 0.1 mm (A–B').

RP58 mutant cortices suggest that RP58 may play a role in neuronal positioning or migration.

The *RP58*-deficient hippocampus was reduced in size and had no identifiable CA pyramidal layer or DG granular layer in sections stained with Nissl (Fig. 1), NeuN (Supplementary Figs. 2G' and H'), or MAP2 and Tuj1 double stain (see Supplementary Figs. 2A–B").

Cajal-Retzius cells play an important role in the normal layer formation of the hippocampus. The Tbr1/reelin double staining revealed that Cajal-Retzius cells (Nakajima et al., 1997), some of which were Tbr1-positive, were present in the mutant (Fig. 2P). The hippocampal fissure, which is characterized by Reelin-positive cells, was poorly developed (asterisk in Figs. 2O and P). In the developing p73$^{-/-}$ hippocampus, the most striking abnormality is the absence of the hippocampal fissure, which suggests a role for p73 in cortical folding (Meyer et al., 2004). Therefore, p73 and Reelin expression were examined at the cortical hem (see Supplementary Fig. 4), which revealed that the expression of p73 and reelin was both normal in *RP58*-deficient cortical hem. We next examined the CA and DG. The pan-hippocampal plate marker, α-crystalline (Funatsu et al., 2004), was expressed in a more dorsal cortical region in the mutant than in the wild type (arrows in Figs. 4A and E). Since α-crystalline is also expressed in the neocortex as well as in the hippocampus, we used another hippocampal marker, α-synuclein, together with the DG marker, Prox1. We found that α-synuclein was expressed in the hippocampal region and its staining did not overlap with the Prox1-positive region in the wild-type brain. In contrast, although α-synuclein expression was detected in the more dorsal cortical region in the mutant brain, it did not overlap with the Prox1-positive dentate region (see Supplementary Figs. 5A–B'"). These results suggested that the hippocampus was formed in a more dorsal region in the mutant, probably because of an insufficiency in hippocampal folding; however, the basic positional relationship between the CA and DG remained intact.

Furthermore, we examined whether specific hippocampal subfields were generated in the *RP58*-deficient mice. The expression of the CA3-specific marker KA1 (Grik4) (Bettler et al., 1990) was almost undetectable (an arrow in Figs. 4B and F). The CA1-specific marker SCIP (Pou3f1) (Frantz et al., 1994; arrows in Fig. 3C) was not detected (Fig. 4G). NT3, which is expressed in the cingulate neopallium (Friedman et al., 1991; Lee et al., 2000; an arrow in Fig. 4D), was also not detected in the mutant (Fig. 4H). To examine the DG, we used Prox1 and NeuroD (Figs. 2Q–T), which are markers of immature dentate granule cells (Pleasure et al., 2000; Galichet et al., 2008). In the wild type, Prox1- and NeuroD-positive cells formed a V-shaped structure, which is typical of the DG, whereas in the mutant they formed an inverted V-shaped structure (arrowhead in Figs. 2Q–T). The DG region that was positive for Prox1 appeared to extend throughout the *RP58* mutant hippocampus (Supplementary Fig. 6), suggesting that loss of RP58 function may result in an increase in the number of Prox1-positive dentate granule cells. It is reported that Tbr1 is expressed after onset of NeuroD expression (Hevner et al., 2006). Tbr1 was expressed in many NeuroD-positive dentate granule cells in the wild type, whereas its expression was severely reduced in the mutant (Figs. 2S and T), suggesting that the production of mature neurons is impaired in the mutant dentate granule cells. These results suggest that, although major areas of the hippocampus were probably retained in the mutant, the CA1, CA3 fields, the cingulate cortex, and DG were not, indicating that the hippocampal neurons had maturation defects like those seen in the neocortex.

Expression pattern of RP58 protein

The abnormality of neurons generated in the mutant cortex indicates that RP58 functions during the development of the neocortex

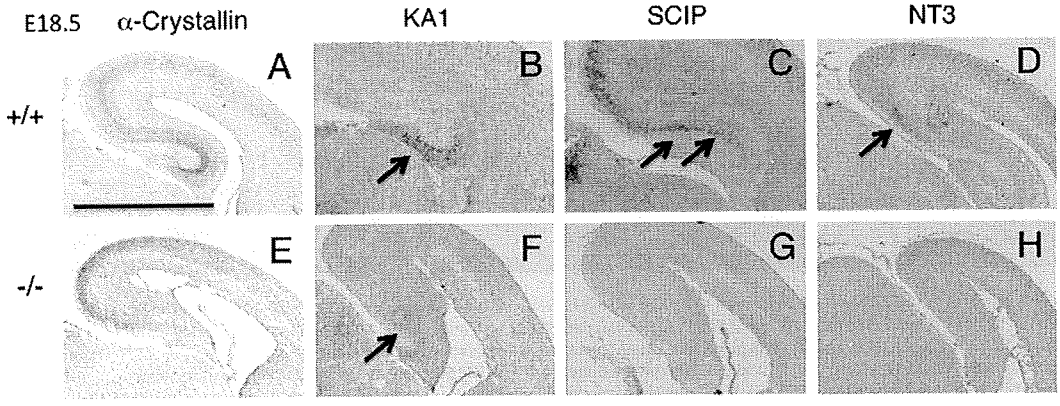

Fig. 4. Field specification impairment in the hippocampus of *RP58*-deficient E18.5 mice. α-crystalline, which is a pan-hippocampal marker, was detected in the hippocampal region of the wild-type brain (arrows in A), whereas it was detected in the more dorsal region in the *RP58*-deficient brain (arrows in E). The expression of the CA3-specific marker KA1 (an arrow in B) was almost not detected in the mutant brain (an arrow in F). In the wild-type brain, SCIP was expressed in CA1 sector of the hippocampus (arrows in C) and in the adjacent cortex, while it was not detected in the mutant brain (G). NT3, which is a cingulate neopallium marker (an arrow in D), was not detected in the mutant (H). Scale bar, 1 mm (A–H).

and of the hippocampus. To further understand the function of RP58, we examined the expression patterns of the RP58 protein using an RP58-specifc antibody (Takahashi et al., 2008). The immunostaining pattern obtained was almost identical to that of the RP58 mRNA *in situ* hybridization pattern (Figs. 5A and B). The specificity of the RP58 antibody was confirmed by immunostaining of an *RP58*$^{-/-}$ brain (Fig. 5C). Double staining using the nuclear marker TOPR3 showed that RP58 was localized in the nucleus and that it was absent from the cytoplasm (Supplementary Figs. 7B and B'''). At E12.5, RP58 was detected in preplate neurons and in some cells in the VZ (arrows in Fig. 5D). At E16.5, RP58 was present in the CP, IZ, SVZ, and in some cells in the VZ (arrows in Figs. 5E and E'), but not in cells of the MZ (Fig. 5E). Double staining with β-synuclein or Reelin indicated that RP58 was expressed in subplate neurons (arrows in Fig. 5F), but not in Cajal-Retzius cells (Fig. 5G; Supplementary Fig. 8). RP58 was not detected in Dlx2-positive cells (arrows in Fig. 5I), which correspond to GABAergic neurons. In the E16.5 hippocampus, RP58 was detected in most developing neurons and in some progenitor cells in the VZ (Fig. 5J). At E18.5, RP58 was detected in migrating neurons, pyramidal layer cells of the CA, and dentate granule cells (Fig. 5K), which were identified by immunoreactivity for NeuroD (Figs. 5L and L'). RP58 was not detected in reelin-positive Cajal-Retzius cells in the hippocampal fissure (asterisk in Fig. 5K). Therefore, RP58 is expressed in migrating and postmigratory glutamatergic neurons, which are impaired in the mutant, whereas RP58 is not expressed in the Cajal-Retzius cells and GABAergic neurons, which are not impaired in *RP58*-deficient animals, as shown in Fig. 2. Interestingly, RP58 is also expressed in the progenitor cells in the VZ. Interestingly, some cells in the VZ expressed the RP58 protein at a high level (arrows in Fig. 5H; Supplementary Figs. 7A–B'''), and other cells expressed this protein at a low level (arrowheads in Supplementary Figs. 7A–B'''). As all of these cells were positive for Ki67, a nuclear protein expressed only in cycling cells, this result suggests that RP58 is expressed by neural progenitors.

To examine whether the VZ cells that express RP58 are RGPs and/or IMPs, we performed double labeling of RP58 with Pax6 (which is an RGP marker) and Tbr2 (which is a pan-IMP marker). Most of the RP58-positive cells in the VZ were Tbr2-positive (arrows in Supplementary Figs. 9C–C'''), whereas some RP58-positive cells were Pax6-positive (arrows in Supplementary Figs. 9A–B''') and the others were Pax6-negative (arrowhead in Supplementary Figs. 9A–B'''). RP58 was expressed in P-H3-positive cells in the basal regions of the VZ, but not in the apical region of the VZ (Supplementary Fig. 10). RP58 was also detected in some of Ngn2-positive cells (Supplementary Fig. 11). These results suggest that the onset of RP58 expression happens during the transition from Pax6-positive cells to Tbr2-positive cells, or, in other words, at the initial stage of IMPs.

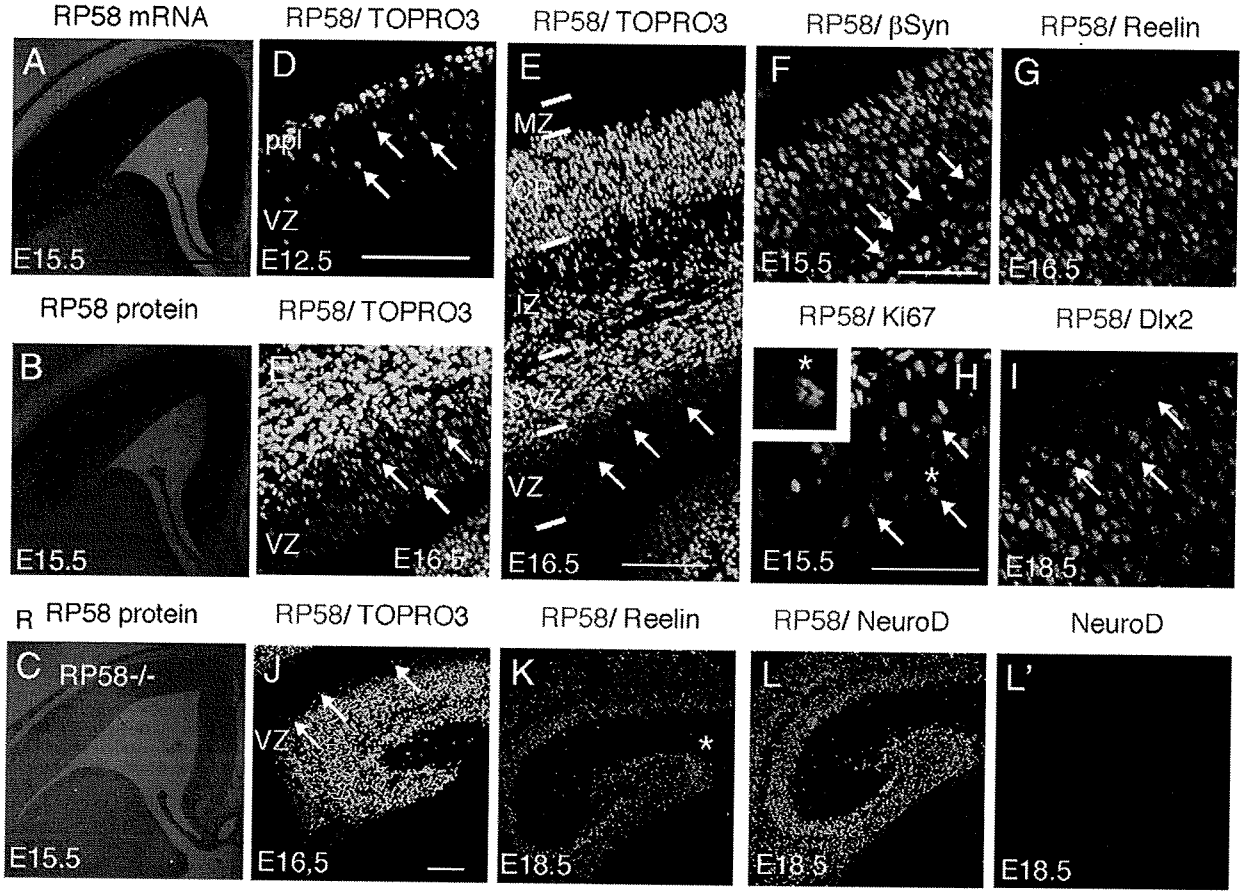

Fig. 5. RP58 expression patterns in the wild-type cerebral cortex. (A) RNA *in situ* hybridization analysis shows that RP58 transcripts were strongly expressed in cortical cells in the CP, IZ, SVZ, and weakly in the VZ of E15.5 wild-type mice. (B and C) RP58 protein was detected at high levels in the CP, IZ, and SVZ, and weakly in the VZ of E15.5 wild-type mice (B). No signal was detected in *RP58*$^{-/-}$ brain (C). (D, E, and E') RP58 protein was intensely expressed in developing neurons in the preplate (ppl) at E12.5 (D), in the CP, IZ, and SVZ at E16.5 (E), and in progenitor cells in the VZ at E12.5 (arrows in D) and E16.5 (arrows in E and E'). (F–I) RP58 was detected in β-synuclein-positive subplate neurons at E15.5 (F) and was not detected in the reelin-positive Cajal-Retzius cells at E16.5 (G). Ki67, which is a cell cycling marker, was detected in RP58-positive cells in the VZ at E15.5 (H). A higher magnification view of the region marked by an arrow with an asterisk (*) indicates that RP58 protein was expressed in Ki67-positive progenitor cells. RP58 was not detected in Dlx2-positive GABAergic neurons in the E18.5 neocortex (I). (J) RP58 was expressed in progenitors cells in the VZ (arrows in J) and in the developing neurons of the E16.5 hippocampus. (K–L') RP58 was not detected in reelin-positive Cajal-Retzius cells in the hippocampal fissure (asterisk, K) at E18.5. RP58 was detected in NeuroD-positive DG granule cells (L, L') at E18.5. Scale bars, 1 mm (A–C); 0.1 mm (D and E'), (E), and (J–L'); and 0.05 mm (F, G and I), (H).

Enhanced apoptosis in the RP58-deficient cortex

Next, we examined whether enhanced cell death or reduced production of cortical neurons in the mutant cortex were responsible for the fewer numbers of mature subplate and specified CP neurons observed in the mutant cortex. A larger number of TUNEL-positive cells were found in the postmitotic zone of the mutant neocortex at E15.5 and E18.5 when compared with the wild type, but no differences were observed in the proliferative zone (Figs. 6A, B, E, and F; Supplementary Fig. 12). The mutant hippocampus displayed a significant increase in the number of TUNEL-positive cells at E18.5 when compared with the wild type (Figs. 6M and N). Active-caspase3 immunoreactivity was also enhanced at E16.5 (Figs. 6C, D, I, and J) and E19 (Figs. 6G, H, O, and P) in both the neocortex and the hippocampus of the mutant mice, which suggests that caspase-dependent apoptosis is enhanced in the mutant. Apoptosis was detected in the anterior and posterior neocortex to the same degree (data not shown). Furthermore, single-strand DNA (ssDNA) staining using an anti-ssDNA antibody documented the presence of fragmented DNA (Figs. 6K and L), which confirmed the results of the TUNEL analysis. These results suggest that *RP58* deficiency enhances caspase-dependent apoptosis in the cerebral cortex, which may reduce the number of mature cortical neurons.

Expansion of the VZ/SVZ in the RP58-deficient cortex

In addition to enhanced apoptosis, we found that the VZ was likely to be expanded in the postnatal day (P) 0 mutant cortex (asterisk in Fig. 1B). We therefore examined the expression of several markers of the VZ, which included Pax6 (Englund et al., 2005). Pax6 expression expanded radially in the mutant cortex at E19 when compared with the distribution of this protein in the wild-type cortex at E19, as did PCNA immunoreactivity (Figs. 7A–B"). Furthermore, the expression of HES5, which is a basic helix–loop–helix transcription repressor expressed in the VZ (Ohtsuka et al., 2006), and of Tailless, which is an orphan nuclear receptor restricted to the VZ (Monaghan et al., 1995), was also enhanced in the mutant neocortex (Figs. 7C–F). The VZ was expanded in the hippocampus as well as in the neocortex, as determined by double staining of Pax6 with PCNA or Ki67 at E18.5 (Supplementary Fig. 13).

Next, we examined whether IMPs were increased in the mutant. Tbr2-positive cells, which are detected in IMPs and postmitotic immature neurons (Englund et al., 2005), were increased in the E18.5 mutant (Supplementary Figs. 14A and B). The phosphohistone H3 (P-H3)-positive mitotic cells in the SVZ, which correspond to mitotic cells of IMPs, were also increased, together with PCNA-positive cells (see Supplementary Figs. 14C–D'). These results suggest that IMPs were

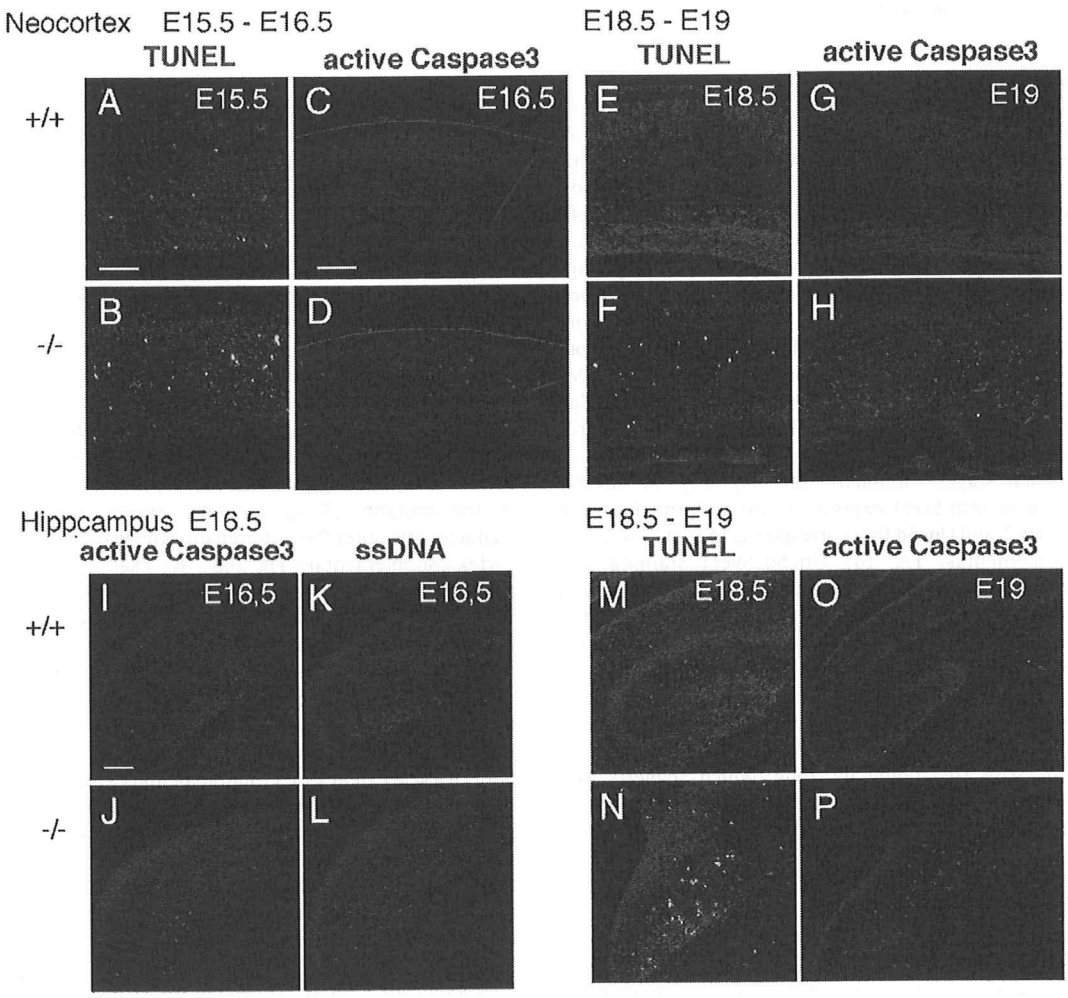

Fig. 6. Enhancement of apoptosis in the *RP58*-deficient cortex. (A–H) In the mutant neocortex, the number of TUNEL-positive cells was higher than in wild type at E15.5 (A and B) and E18.5 (E and F), and the number of active-caspase 3-positive cells was higher at E16.5 (C and D) and E19 (G and H). (I–P) In the mutant hippocampus, active-caspase 3-positive cells (I and J) and ssDNA-positive cells (K and L) were increased at E16.5 and TUNEL-positive cells and active-caspase 3-positive cells were also increased at E18.5 (M–P). Scale bars, 0.1 mm (A, B, E, F, M, and N), (C, D, G, H, O and P), and (I–L).

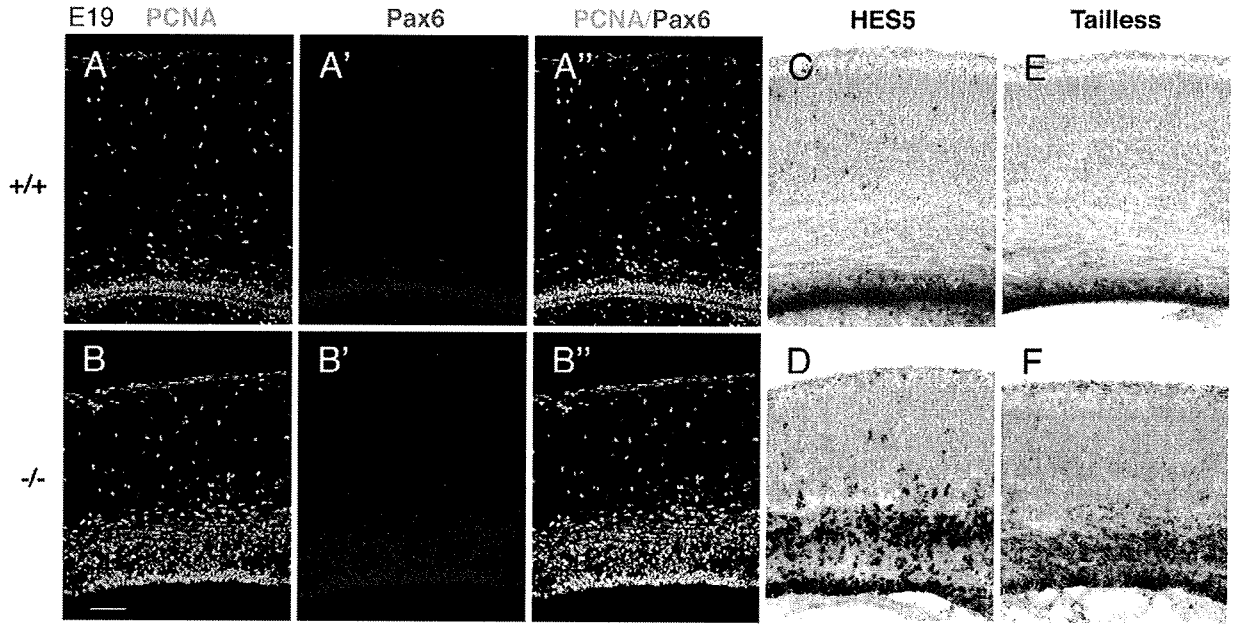

Fig. 7. Expansion of the ventricular zone in the *RP58*-deficient cortex. (A–B") PCNA-positive cells and Pax6-positive cells were increased in the $RP58^{-/-}$ cortex (A–B') and most Pax6-positive cells were immunoreactive for PCNA (A" and B"). (C–F) The $RP58^{-/-}$ cortex (D and F) exhibited more HES5-positive cells (C and D) and Tailless-positive cells (E and F) than the wild-type cortex (C and E). Scale bar, 0.1 mm (A–F).

increased in the mutant. To examine the developmental stage of IMPs, we performed double staining of Tbr2 and Pax6 (Fig. 8), as Pax6+/Tbr2+ cells and Pax6−/Tbr2+ cells are early-stage IMPs and late-stage IMPs, respectively (Sasaki et al., 2008). The double staining revealed that, in the E18.5 mutant, Tbr2-positive cells and Pax6-positive cells were increased in number, that both Pax6+/Tbr2− cells and Pax6+/Tbr2+ cells were also increased, whereas Pax6−/Tbr2+ cells were not (Fig. 8). This result suggests that RGPs and early-stage IMPs were increased in the mutant, whereas late-stage IMPs were not. To examine the identify of the SVZ, we preformed Svet1 *in situ* hybridization near the section of the Pax6/Tbr2 double staining from E15.5 to E18.5, which revealed that impairment of the mutant VZ/SVZ progressed from E15.5 to E18.5 (Supplementary Fig. 15). In particular, a tripartite appearance of inner Pax6-dominant/intermediate Tbr2-dominant/outer Pax6-dominant zones was observed in the mutant in later developmental stages (Supplementary Fig. 15). To directly associate these zones with Svet1 expression, we performed a triple staining of Pax6, Tbr2, and Unc5d that corresponds to Svet1 (Sasaki et al., 2008) (Supplementary Fig. 16). Unc5d/Svet1 staining was detected in the upper region of the Tbr2-positive zone in the wild type, while it was also detected, albeit weakly and diffusely, in the upper region of the intermediate Tbr2-positive zone and contained the outer Pax6-dominant zones in the E16.5 mutant mice (Supplementary Figs. 16 A–B'), which suggests that the outer Pax6-dominant zone was located in the SVZ. In the E18.5 mutant, the expression of Unc5d/Svet1 was more diffusely detected in the outer Pax6-dominant/intermediate Tbr2-dominant zone, which suggests that the mutant VZ/SVZ was severely impaired in the late development stages of the mutant (Supplementary Figs. 16 C–D').

The impairment of cell-cycle exit in the RP58-deficient VZ/SVZ during late development

We next examined whether the expansion of the VZ/SVZ of the mutant cortex was due to enhanced proliferation and/or impairment of cell-cycle exit. To examine cell proliferation, we counted the number of BrdU-labeled cells in a random selection of 50 Ki67 (which is a proliferating cell marker)-positive cells (which are considered to be progenitor cells) after a 30 min pulse of BrdU. The percentage of progenitor cells labeled with BrdU was not altered in the mutant cortex at E15.5, which suggests that proliferation was not altered in the mutant cortex (Figs. 9A–C). To examine the possibility that the division pattern of progenitor cells was impaired in the mutant cortex, we counted the number of PCNA-negative and Pax6-negative cells in a random selection of 50 BrdU-labeled cells, after a 24 h pulse of BrdU; this corresponds to the fraction of cells exiting the cell cycle. At E16.5, we found that the PCNA−/BrdU+ and Pax6−/BrdU+ ratios were about halved in *RP58* mutant progenitor cells when compared with their normal counterparts, which suggests that cell-cycle exit is inhibited in the mutant VZ progenitor cells in both the medial and lateral neocortices (Figs. 9D–I). This was confirmed by examining the total number of BrdU-positive cells in an area of 0.25 mm^2, which showed an increase in the number of PCNA− or Pax6+ cells; this suggests that reentry into the cell cycle is enhanced in the mutants (Supplementary Fig. 17). Furthermore, as the characteristic outer Pax6-dominant zone was observed in the mutant cortex (Supplementary Fig. 16B), we examined whether the outer Pax6-dominant zone was involved in the reduction of cell-cycle exit. The Pax6−/BrdU+ ratio was dominantly reduced in the upper region (IZ/SVZ), which contained the abnormal outer Pax6-dominant, when compared with the lower region (VZ) (Supplementary Fig. 18). Therefore, it is possible that the abnormal outer Pax6-dominant zone observed in the mutant reflects the reduction of cell-cycle exit. In contrast, neither proliferation at E12.5 (Supplementary Figs. 19A–C) nor cell-cycle exit at E13.5 (Supplementary Figs. 19D–I) was impaired. These results suggest that cell-cycle exit is reduced in the mutant cortex at late neocorticogenesis. The reduction of the cell-cycle exit causes an increase in VZ progenitor cells and thereby leads to the expansion of the VZ. Therefore, it is likely that the reduction of cell-cycle exit, in addition to the enhanced apoptosis, decreases the number of differentiated late-born neurons in the mutant CP.

As cell-cycle kinetics may affect cell-cycle exit, we estimated the duration of the S-phase (Ts) and of the total cell-cycle time (Tc) using a BrdU/IdU double labeling paradigm (Martynoga et al., 2005), which revealed no obvious differences in Ts, Tc, and Ts/Tc between wild-type and mutant cortices (Supplementary Fig. 20); however, because this

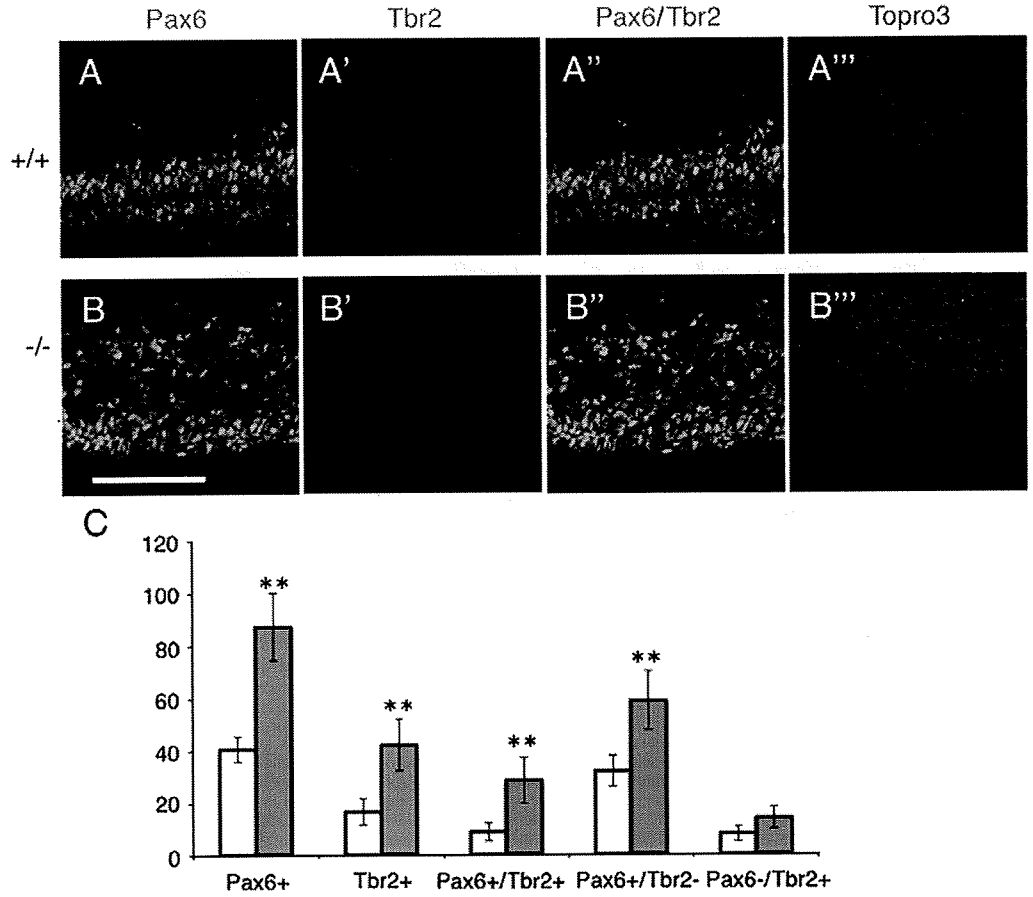

Fig. 8. Both Pax6-positive and Tbr2-positive cells were increased in the *RP58*-deficient cortex. Double staining (A", B") of Pax6 (A, B) and Tbr2 (A', B') with the TOPRO3 nuclear stain (A'", B'") showed that both Pax6-positive and Tbr2-positive cells were increased in the *RP58*-deficient cortex. Scale bars, 0.1 mm (A–B"). (C) The number of Pax6+, Tbr2+, Pax6+/Tbr2+, Pax6+/Tbr2−, and Pax6−/Tbr2+ cells was counted in a 0.0083 mm^2 area of the wild-type (open column) and of the mutant neocortex (gray column). Faint staining of Pax6 was regarded as negative. Six regions of three mutant brains were compared with six regions of three wild-type brains. The data are presented as means ± SD. $^{**}P<0.01$ (Student's *t* test).

estimation rested on the assumption that all cells in the VZ are proliferating and that the precursor cells consist of a single proliferating population with the same cycling kinetics (Martynoga et al., 2005), further analyses may be necessary to assess the possibility that RP58 is involved in cell-cycle kinetics.

Discussion

In the present study, we characterized mice carrying disrupted alleles for the POZ/zinc finger transcriptional repressor gene, *RP58*. We found that homozygous mutants display severe hypoplasia of the cerebral cortex and of the hippocampus, in association with enhanced apoptosis and expansion of the VZ/SVZ. We showed that RP58 is specifically required for the maturation and survival of the excitatory neurons of the cerebral cortex. Furthermore, the present study demonstrated that RP58 is a novel factor that controls the balance of cell division of neuronal progenitors, which remains poorly understood to date.

In the *RP58* null mutant, the VZ was expanded and the dorsal cortex appeared like a wild-type younger brain. Therefore, the possibility of developmental delay cannot be excluded. We examined the expression of Tbr1 in the mutant cortex at E13.5, E15.5, and E18.5, which suggested that there is no clear time lag in the Tbr1 expression pattern (Supplementary Fig. 3). In addition, the Tc may cause a developmental delay. The Tc was not altered in the *RP58*-deficient mice (Supplementary Fig. 20). These results do not support the contention that developmental delay mainly occurs in *RP58* null mice. It seems more likely that reduction of produced matured neurons and enhancement of apoptosis causes the impairment in cortical development observed in these animals.

One of the main phenotypes in the *RP58*-deficient cortex was a reduction in the number of mature cortical neurons. In addition to a substantial reduction in the number of neurons in the subplate and layers 2–5 of the CP in the neocortex, Tbr1 expression was strongly suppressed throughout the cortical anlage, with the exception of the Cajal-Retzius cells in the hippocampus. The pyramidal layer of the CA was absent and Tbr1 expression was severely reduced in NeuroD-positive granule cells of the DG. NeuroD is expressed after Pax6, but before Tbr1 (Hevner et al., 2006), which suggests that *RP58* deficiency suppresses the production of mature dentate granule neurons.

In the early embryonic stage, *RP58* deficiency did not impair cell-cycle exit, although apoptosis was enhanced in the mutant neocortex at E15. Therefore, the decreased number of mature subplate neurons produced at early embryonic stages could be caused by enhanced apoptosis. On the other hand, the VZ was expanded at later embryonic stages in the mutant, the cell-cycle exit was inhibited in RGPs, and the level of apoptosis remained high, which suggest that enhanced apoptosis and/or defective cell-cycle control reduce the production of mature cortical neurons at later development stages.

Transgenic mice expressing β-catenin precursors also show reduced cell-cycle exit and develop enlarged brains with reduced cortical thickness (Chenn and Walsh, 2002). In contrast, $RP58^{-/-}$ mice showed no enlargement of the brain, although the thickness of the neocortex was reduced. This discrepancy may be due to the reduction